

Editor's comment

First of all, apologies for my delay in handling this manuscript. I have now received two reviews of your re-revised manuscript. Both reviewers find the paper improved, and I agree with their evaluation. Inclusion of the idealised case (as suggested by reviewers) has also benefited the paper.

The first reviewer, who is not a modeller, finds the paper improved and recommends minor revision. The second reviewer, however, raises some major issues regarding the errors in both the surface mass balance and ice flow model, and I agree with his main three points. These are major issues that jeopardise the quality of your paper.

I therefore recommend major revisions.

Since this is the third iteration in a process that has taken a long time, I suggest that you make a real effort to address those points. I would be happy to discuss with you the needed revisions, and I am sure that the reviewer, Martin Truffer, who has decided from the beginning not to be anonymous, would also be happy to discuss this with you.

I really think this is a nice paper that would be worth publishing, but the main issues related to errors should be addressed in a satisfactory manner. Please get back to me and/or the reviewer if we can help you with the revision, so that the paper will get to a prompt conclusion soon.

*Non-public comments to the Author:
Dear Koji and co-authors,*

This is an addition for you only. Again, apologies for my delay in handling this manuscript.

Please see above for my recommendation, which is a major revision again, based on the comments of the second reviewer, who did a very thorough job and is an expert on the flow modeling and the main topics of the paper. His three main issues are all important and you need to address them properly.

Since this is the third iteration in a process that has taken a long time (partly because of my absences, and partly because not all issues were always satisfactorily addressed), I suggest that you make a real effort to address those points. I would be happy to discuss with you the needed revisions, and I am sure that the reviewer, Martin Truffer, who has decided from the beginning not to be anonymous, would also be happy to discuss this with you.

If the revision is not satisfactory this time, my suggestion will be to reject the paper and encourage a new resubmission here or elsewhere.

You might remember that I had sent a separate email to you after the last revision asking to improve the way you responded to some of the issues raised by the reviewers.

I really think this is a nice paper that would be worth publishing, but the main issues related to errors should be addressed in a satisfactory manner.

Please get back to me and/or the reviewer if we can help you with the revision, so that the paper will get to a prompt conclusion soon.

Reply to referee comments

We would like to thank two referees for thoughtful and useful comments. In the following, we describe our responses (in blue) point-by-point to each referee comment (*italic*). The revised manuscript was edited by Stallard Scientific, an English editing company in New Zealand (<https://www.stallardediting.com/>).

Reviewer #4

This is the third review of Tsutaki et al.'s manuscript. The manuscript is much improved again. As I am not a modeller, I have been largely unable to comment on the modelling section, however, I think the changes made based on the suggestions of Reviewer 5 to present the modelling as an idealised case has helped mitigate issues with the large uncertainties I had previously pointed out. I do think the idealised case should be restated in the conclusions section. Otherwise I have only a few minor comments, which I list below.

[Reply] Thanks a lot for the detailed comments and suggestions.

Specific comments:

L16: change “glacier” to “glaciers”

L38: “monsoonal” rather than “monsoon-influenced”?

L55 and thereon: no space between a number and % sign

L80: suggest combining these sentences – “contrasting termini at similar elevations, which makes them...”

L131 and thereon: no dash between a number and m (denoting metres) – this has become inconsistent through the text and figure captions

L172: remove “the areal” (repetition of area)

L204-5: shortwave and longwave should be one word

L219 and thereon: no space between a number and degree sign

L230: add “the” before “debris-covered”

L240: add “the” before “melting”

L304: “smoothing the elevations” rather than “filtering the elevations with a smoothing routine”?

L315: remove “and” before “several”, and “numbers” should be “number”

L404: “reversed” instead of “prescribed” for consistency with earlier in manuscript

L415: remove “within”

L430: add “to be” after “considered”

L540: hyphenate “water-saturated”

[Reply] All comments above were corrected according to the reviewers' suggestions.

L295: I still have issue with: i) the assumption of temperate conditions, and ii) the apparent (and later contradictory) assumption of no basal sliding in the modelling (L319). First, I don't see how the air temperature over a lake determines the temperature of a glacier? Lakes obviously have a temperature $> 0^{\circ}\text{C}$ unless they are frozen through (which still wouldn't represent the glacier's thermal regime), and can additionally alter the local microclimate (Carrivick and Tweed, 2013), and I therefore don't think this is a valid assumption. Second, if you do assume temperate conditions, there WILL be (at least some) basal sliding – which your results show (L427). The clause “We assumed no basal sliding” (L319) is thus unclear (at least to a non-modeller) and needs to be altered.

[Reply] We calculate ice thickness of both glaciers to reproduce observed surface velocity distribution with assuming a frozen bed (no basal sliding and warm and soft ice), and then obtain 800 and 300 m for Thorthormi and Lugge glaciers, respectively. These are much greater than the observational lake depth (~ 100 m). In particular, with almost flat surface and fast flow, Thorthormi would have an extremely thick ice. We briefly address this in the text.

For issue ii), we removed the sentence “We assumed no basal sliding, and” and changed here as “We applied a fourth-order...” to be clear the fact that we applied basal sliding in the model.

L380: is this flow uncertainty ± 12.1 or ± 6.05 m/a?

[Reply] Uncertainty is estimated to be ± 12.1 m a⁻¹. We added plus-minus sign before 12.1 in the revised manuscript.

L475-6: if the difference between these glaciers and others in Nepal are similar, how can the role of ice dynamics be different?

[Reply] We deleted this sentence because a point of discussion is unclear here.

L505: I'd be careful with this use of “thickening”, as the overall thinning rate is still negative – this clause implies to me that the thickening is greater than the negative SMB. This is expressed better in the final sentence of this paragraph, so I would suggest either wording more carefully (akin to L512) or just removing this final clause after “emergence velocity”. Similar for L23 – perhaps change “suppressed” to “minimised”?

[Reply] We deleted this sentence “and therefore thickening to compensate for the negative SMB” because this is described more clearly in the latter part of this section as reviewer suggested. We changed “suppressed” to “minimized” in the abstract.

Carrivick, J. L. and Tweed, F. S.: Proglacial Lakes: Character, behaviour and geological importance, *Quat. Sci. Rev.*, 78, 34–52, doi:10.1016/j.quascirev.2013.07.028, 2013.

Reviewer #5

This paper has improved a lot since its last iteration, particularly in grammar and language, which helps a lot with understanding. As I've stated before, the topic of the paper is interesting, the findings are significant, and I do hope that this will be published.

Unfortunately I still think that there are some issues that need to be addressed, and these issues revolve around the treatment of errors in both SMB and the flow model. I am not certain what the correct way is to address these errors, but the way it is done here is incorrect.

For the SMB the authors use the standard deviation of the SMB over the modelled area as an estimate of error. This is clearly incorrect, the spatial variability of modelled SMB is entirely unrelated to the error. A better way to estimate error would be if there are any independent estimates to compare to (even over short times), but this might not exist? Or a comparison of integrated SMB to geodetic balance for a land terminating glacier.

[Reply] We agree with this comment. However, there is no data to compare with our SMB estimate. Although we have conducted DGPS surveys at a land-terminating glacier (Lugge 2) for the studied period, the domain is limited to the debris-covered ablation zone where the surface lowering is also affected by glacier dynamics. We will encounter the same problem argued by reviewers because of no thickness data. If this "geodetic balance" means "glacier-wide mass balance", on the other hand, we can compare our SMB estimate with some remotely sensed mass balance. However, we concern that large uncertainty for the accumulation zone in both remote sensing analysis and model estimate would not support justification of the model. Therefore, we will simply replace the standard deviation (spatial variability of SMB) by the error estimated by changing related parameters (Figs. S12 and S13). Because SMB of the debris-covered ablation zone is equal to melt amount with negative sign, we will show spatial averages of uncertainties (Fig. S13) as SMB errors (± 2.92 m w.e. for Thorthormi and ± 2.41 m w.e. for Lugge glaciers).

For the flow model, the stated error is clearly not correct, because measurements of velocity and simulated thickness change are outside the error range. There are a number of issues with modeled ice velocities that have yet to be addressed:

1) *The issue of 'apparent mass balance' has not been addressed in the revision. This quantity is the $SMB - dh/dt$ in the Farinotti paper. A negative thickness change contributes to mass flux and works opposite the SMB. In this case thickness changes are almost of the same magnitude as SMB, so the 'apparent mass balance' is much closer to zero, which would have an important effect on the calculated ice thickness.*

[Reply] In the former version of the revised manuscript, we calculated apparent mass balance by the simulated SMB and dh/dt observed by ASTER DEMs. However, we described in the manuscript as "with ... and the above-mentioned SMB model (Sect. 3.4)", leading to misunderstanding for reviewer that we did not calculate apparent mass balance. In the revised manuscript, we changed a description to "above-mentioned SMB model (Sect. 3.4) and satellite-based ice thickness change (Sect. 3.1)".

2) *The calculated emergence velocities show some clear errors, for example, the large positive values in Fig. 5b. If those were correct, the glacier would be thickening in those places at fast rates; this is not observed. I think that errors in emergence velocities are simply too large to say something meaningful about simulated thickness changes. It would make more sense to calculate emergence velocities from observed thickness change and modelled SMB.*

[Reply] We agree that errors in emergence velocities are still too large to discuss simulated thickness changes for experiments 1 and 2. As reviewer pointed out in the latter comment, comparing the results between experiments 1 and 2 is important for our conclusion. We addressed spatial variation of sliding coefficients in the flow model to reproduce observed velocities more accurately. Sliding coefficients were determined by minimizing of RMSE between modelled and measured surface flow velocities over the area within 4100 m and 500-1900 m of the termini of Thorthormi and Lugge glaciers, respectively. Obtained distribution of the sliding coefficient (C) is shown in Figure S5. Based on these new results, emergence velocities were re-calculated for experiments 1 and 2. We added Figure 8 to compare longitudinal distribution of emergence velocities calculated from experiments 1 and 2.

3) Both Thorthormi and Lugge Glaciers show step changes in observed velocities that are not at all reproduced in the model.

[Reply] There is one possibility that step changes in observed surface velocities are due to miscorrelation in feature tracking process caused by surface ogives along the center of both glaciers. In the revised manuscript, we simulated emergence velocities over the area within 4100 m of the terminus of Thorthormi and within 500-1900 m of the terminus of Lugge Glacier, where step changes in velocities were not observed. We added the description “Measured surface velocities show step changes at 800–1200 m and 1900–2000 m from the termini of Thorthormi and Lugge glaciers, respectively (Fig. 3). It is likely that these step changes are due to miscorrelation in feature tracking process caused by surface ogives along the centre of the glaciers. Consequently, we only interpret the simulated velocities within 500–1900 m of the terminus of Lugge Glacier. For Thorthormi Glacier, we considered a mean value of observed velocities at the area as a reference value of simulation.” in Sect. 4.5.3.

These inadequacies are perhaps not such a big surprise. There are many things that the model does not consider, such as the influence of lateral stresses or spatial variation of sliding coefficients. The latter could be addressed, but in some sense the goal here is not to reproduce velocities. Rather, the authors should stress the changes that occur between experiment 1 and 2.

[Reply] We removed simulated thickness changes in the revised manuscript because those uncertainties are still too large to compare with observed thickness changes. We addressed spatial variation of sliding coefficients in the flow model as described above reply.

Smaller comments:

The thinning rate is sometimes stated as a positive number (1.114/115) and sometimes as a negative number (1.17/18). It is generally clear from the context what is meant, but you should at least be consistent. My preference is to always use thickness change, rather than thinning rate.

[Reply] We changed “thinning rate” to “thickness change” throughout the manuscript.

My previous comment about partial derivatives was slightly misunderstood: In eqn 14, you should use partial derivatives for h ; this is an equation that is valid at each point in

time. Otherwise, I like the changes, that is, measurements are now all referred to by $\Delta z / \Delta t$. I think that's the most accurate representation. Basically what you do is to take a measurement $\Delta z / \Delta t$ as an estimate for the quantity $\partial h / \partial t$.
[Reply] We agreed using $\Delta z / \Delta t$ throughout the manuscript.

These comments are all addressable and I do hope that the paper can be published. I also apologize for the delay with the review; it came at a very busy time.
[Reply] Thanks a lot for your careful review for many times. Our manuscript is now much improved from the original one.

1 **Contrasting thinning patterns between lake- and land-terminating** 2 **glaciers in the Bhutan Himalaya**

3 Shun Tsutaki^{1,a}, Koji Fujita¹, Takayuki Nuimura^{1,b}, Akiko Sakai¹, Shin Sugiyama², Jiro Komori^{1,3,c},
4 and Phuntsho Tshering^{1,3,d}

5 ¹Graduate School of Environmental Studies, Nagoya University, Nagoya, Japan

6 ²Institute of Low Temperature Science, Hokkaido University, Sapporo, Japan

7 ³Department of Geology and Mines, Ministry of Economic Affairs, Thimphu, Bhutan

8 ^anow at: Atmosphere and Ocean Research Institute, The University of Tokyo, Kashiwa, Japan

9 ^bnow at: ~~Chiba Institute of Science, Choshi~~ [Tokyo Denki University, Hatoyama](#), Japan

10 ^cnow at: Department of Modern Life, Teikyo Heisei University, Tokyo, Japan

11 ^dnow at: Cryosphere Services Division, National Center for Hydrology and Meteorology, Thimphu, Bhutan

12 *Correspondence to:* Shun Tsutaki (tsutshun@frontier.hokudai.ac.jp) and Koji Fujita (cozy@nagoya-u.jp)

13 **Abstract.** Despite the importance of glacial lake development in ice dynamics and glacier thinning, in situ and satellite-based
14 measurements from lake-terminating glaciers are sparse in the Bhutan Himalaya, where a number of proglacial lakes exist. We
15 acquired in situ and satellite-based observations across lake- and land-terminating debris-covered ~~glacier~~ [glaciers](#) in the Lunana
16 region, Bhutan Himalaya. A repeated differential global positioning system survey reveals that ~~thinning~~ [thickness change](#) of
17 the debris-covered ablation area of the lake-terminating Lugge Glacier ($-4.67 \pm 0.07 \text{ m a}^{-1}$) is more than three times
18 ~~greater~~ [negative](#) than that of the land-terminating Thorthormi Glacier ($-1.40 \pm 0.07 \text{ m a}^{-1}$) for the 2004–2011 period. The
19 surface flow velocities decrease down-glacier along Thorthormi Glacier, whereas they increase from the upper part of the
20 ablation area to the terminus of Lugge Glacier. Numerical experiments using a two-dimensional ice flow model demonstrate
21 that the rapid thinning of Lugge Glacier is driven by both a negative surface mass balance and dynamically induced ice thinning.
22 However, the thinning of Thorthormi Glacier is ~~suppressed~~ [minimised](#) by a longitudinally compressive flow regime. ~~The~~
23 ~~magnitude of dynamic thickening compensates approximately two third of the negative surface mass balance of Thorthormi~~
24 ~~Glacier.~~ Multiple supraglacial ponds on Thorthormi Glacier have been expanding since 2000 and merged into a single
25 proglacial lake, with the glacier terminus detaching from its terminal moraine in 2011. Numerical experiments suggest that the
26 thinning of Thorthormi Glacier will accelerate with continued proglacial lake development.

27 **1 Introduction**

28 The spatially heterogeneous shrinkage of Himalayan glaciers has been revealed by in situ measurements (Yao et al., 2012;
29 Azam et al., 2018), satellite-based observations (Bolch et al., 2012; Kääb et al., 2012; Brun et al., 2017), mass balance and
30 climate models (Fujita and Nuimura, 2011; Mölg et al., 2014), and a compilation of multiple methods (Cogley, 2016). Glaciers
31 in Bhutan in the southeastern Himalayas have experienced significant shrinkage and thinning over the past four decades. For

32 example, the glacier area loss in Bhutan was $13.3 \pm 0.1\%$ between 1990 and 2010, based on repeated decadal glacier inventories
33 (Bajracharya et al., 2014). Multitemporal digital elevation models (DEMs) revealed that the glacier-wide mass balance of
34 Bhutanese glaciers was -0.17 ± 0.05 m w.e. a^{-1} during 1974–2006 (Maurer et al., 2016) and -0.22 ± 0.12 m w.e. a^{-1} during
35 1999–2010 (Gardelle et al., 2013). Bhutanese glaciers are inferred to be particularly sensitive to changes in air temperature
36 and precipitation because they are affected by ~~monsoon-influenced~~monsoonal, humid climate conditions (Fujita and Ageta,
37 2000; Fujita, 2008; Sakai and Fujita, 2017). For example, the mass loss of Gangju La Glacier in central Bhutan was much
38 greater than those of glaciers in the eastern Himalaya and southeastern Tibet between 2003 and 2014 (Tshering and Fujita,
39 2016). It is therefore crucial to investigate the mechanisms driving the mass loss of Bhutanese glaciers to provide further
40 insight into glacier mass balance (Zemp et al., 2015) and improve projections of global sea level rise and
41 glacier evolution (Huss and Hock, 2018).

42 In recent decades, glacial lakes have formed and expanded at the termini of retreating glaciers in the Himalayas (Ageta
43 et al., 2000; Komori, 2008; Fujita et al., 2009; Hewitt and Liu, 2010; Sakai and Fujita, 2010; Gardelle et al., 2011; Nie et al.,
44 2017). Proglacial lakes can form via the expansion and coalescence of supraglacial ponds, which form in topographic lows
45 and surface crevasses fed via precipitation and surface meltwater. Proglacial lakes are dammed by terminal and lateral moraines,
46 or stagnant ice masses at the glacial front (Sakai, 2012; Carrivick and Tweed, 2013). The formation and expansion of proglacial
47 lakes accelerates glacier retreat through flotation of the terminus, increased calving, and ice flow (e.g., Funk and Röthlisberger,
48 1989; Warren and Kirkbride, 2003; Tsutaki et al., 2013). ~~The ice thinning rates~~Ice thickness changes of lake-terminating
49 glaciers are generally ~~greater~~more negative than those of neighbouring land-terminating glaciers in the Nepal and Bhutan
50 Himalayas (Nuimura et al., 2012; Gardelle et al., 2013; Maurer et al., 2016; King et al., 2017). Increases in ice discharge and
51 surface flow velocity at the glacier terminus cause rapid thinning due to longitudinal stretching, known as dynamic thinning.
52 For example, dynamic thinning accounted for 17-% of the total ice thinning at lake-terminating Yakutat Glacier, Alaska, during
53 2007–2010 (Trüssel et al., 2013). Therefore, it is important to quantify the contributions of dynamic thinning and surface mass
54 balance (SMB) to evaluate ongoing mass loss and predict the future evolution of lake-terminating glaciers in Bhutan.

55 Two-dimensional ice flow models have been utilised to investigate the dynamic thinning of marine-terminating outlet
56 glaciers (Benn et al., 2007a; Vieli and Nick, 2011), which require the ice flow velocity field and glacier thickness. In Bhutan,
57 ice flow velocity measurements have been carried out via remote sensing techniques with optical satellite images (Kääb, 2005;
58 Bolch et al., 2012; Dehecq et al., 2015) and in situ global positioning system (GPS) surveys (Naito et al., 2012), where no ice
59 thickness data are available. Another approach to investigate the relative importance of ice dynamics in glacier thinning is to
60 compare lake- and land-terminating glaciers in the same region (e.g., Nuimura et al., 2012; Trüssel et al., 2013; King et al.,
61 2017).

62 Widespread thinning of Himalayan glaciers has been revealed by differencing multitemporal DEMs constructed from
63 satellite image photogrammetry (e.g., Gardelle et al., 2013; Maurer et al., 2016; Brun et al., 2017). Unmanned autonomous
64 vehicles (UAVs) have recently been recognised as a powerful tool to obtain higher-resolution imagery than satellites, and can
65 therefore resolve the highly variable topography and ~~thinning rates~~elevation changes of debris-covered surfaces more

66 accurately (e.g., Immerzeel et al., 2014; Vincent et al., 2016). Repeat differential GPS (DGPS) measurements, which are
67 acquired with centimetre-scale accuracy, also enable us to evaluate elevation changes of several metres (e.g., Fujita et al.,
68 2008). Although their temporal and spatial coverage can be limited, repeat DGPS measurements have been successfully
69 acquired to investigate the surface elevation changes of debris-free glaciers in Bhutan (Tshering and Fujita, 2016) and the
70 Inner Tien Shan (Fujita et al., 2011).

71 This study aims to reveal the contributions of ice dynamics and SMB to the thinning of adjacent land- and lake-terminating
72 glaciers. To investigate the importance of glacial lake formation and expansion on glacier thinning, we measured surface
73 elevation changes on a lake-terminating glacier and a land-terminating glacier in the Lunana region, Bhutan Himalaya.
74 Following a previous report of surface elevation measurements from a DGPS survey (Fujita et al., 2008), we repeated the
75 DGPS survey on the lower parts of land-terminating Thorthormi Glacier and adjacent lake-terminating Lugge Glacier.
76 Thorthormi and Lugge ~~Glaciers~~glaciers were selected for analysis because they have contrasting termini at similar elevations.
77 ~~These contrasting conditions at similar elevations make,~~ makes them suitable for evaluating the contribution of ice dynamics
78 to the observed ice thickness changes. The glaciers are also suitable for field measurements because of their relatively safe ice-
79 surface conditions and proximity to trekking routes. We also performed numerical simulations to evaluate the contributions of
80 SMB and ice dynamics to surface elevation changes. However, due to lack of observational data for model validation, the
81 models were only used to demonstrate the differences between lake- and land-terminating glaciers using the idealised case of
82 how a proglacial lake can alter glacier ~~thinning rates~~thickness changes.

83 2 Study site

84 This study focuses on two debris-covered glaciers (Thorthormi and Lugge ~~Glaciers~~glaciers) in the Lunana region of northern
85 Bhutan (Fig. 1a, 28°06' N, 90°18' E). Thorthormi Glacier covers an area of 13.16 km², based on a satellite image from 17
86 January 2010 (Table S1, Nagai et al., 2016). The ice flows to the south in the upper part and to the southwest in the terminal
87 part of the glacier at rates of 60–100 m a⁻¹ (Bolch et al., 2012). The surface is almost flat (<1°) within 3000 m of the terminus.
88 The ablation area thinned at a rate of -3 m a⁻¹ during the 2000–2010 period (Gardelle et al., 2013). Large supraglacial lakes,
89 which are inferred to possess a high potential for outburst flooding (Fujita et al., 2008, 2013), have formed along the western
90 and eastern lateral moraines via the merging of multiple supraglacial ponds since the 1990s (Ageta et al., 2000; Komori, 2008).
91 The front of Thorthormi Glacier was still in contact with the terminal moraine during our field campaign in September 2011,
92 but the glacier was completely detached from the moraine in the Landsat 7 image acquired on 2 December 2011. Thorthormi
93 Glacier is therefore termed a land-terminating glacier in this study.

94 Lugge Glacier is a lake-terminating glacier with an area of 10.93 km² in May 2010 (Table S1, Nagai et al., 2016). The
95 mean surface slope is 12° within 3000 m of the terminus. A moraine-dammed proglacial lake has expanded since the 1960s
96 (Ageta et al., 2000; Komori, 2008), and the glacier terminus retreated by ~~~~~1 km during 1990–2010 (Bajracharya et al., 2014).
97 Lugge Glacier thinned near the terminus at a rate of -8 m a⁻¹ during 2000–2010 (Gardelle et al., 2013). On 7 October 1994,

98 an outburst flood, with a volume of $17.2 \times 10^6 \text{ m}^3$, occurred from Lugge Glacial Lake (Fujita et al., 2008). The depth of Lugge
99 Glacial Lake was 126 m at its deepest location, with a mean depth of 50 m, based on a bathymetric survey in September 2002
100 (Yamada et al., 2004).

101 Although the debris thickness was not measured during the field campaigns, there were regions of debris-free ice across
102 the ablation areas of Thorthormi and Lugge ~~Glaciers~~glaciers (Fig. S1). Debris cover is therefore considered to be thin across
103 the study area. Furthermore, few supraglacial ponds and ice cliffs were observed across the glaciers. Satellite imagery shows
104 that the surface is heavily crevassed in the lower ablation areas, suggesting that surface meltwater drains immediately into the
105 glaciers.

106 Meteorological and glaciological in situ observations were acquired across the glaciers and lakes in the Lunana region
107 from 2002 to 2004 (Yamada et al., 2004). Naito et al. (2012) reported changes in surface elevation and ice flow velocity along
108 the central flowline in the lower parts of Thorthormi and Lugge glaciers for the 2002–2004 period. The ice ~~thinning~~
109 ~~rate~~thickness change at Lugge Glacier was ~~~~~approximately -5 m a^{-1} during 2002–2004, which is much ~~higher~~more negative
110 than that at Thorthormi Glacier (~~0-~~less than -3 m a^{-1}). The surface flow velocities of Thorthormi Glacier decrease down-
111 glacier from ~~~~~90 to ~~~~~30 m a^{-1} at 2000–3000 m from the terminus, while the surface flow velocities of Lugge Glacier are
112 nearly uniform at $40\text{--}55 \text{ m a}^{-1}$ within 1500 m of the terminus (Naito et al., 2012).

113 3 Data and methods

114 3.1 Surface elevation change

115 We surveyed the surface elevations in the lower parts of Thorthormi and Lugge glaciers from 19 to 22 September 2011, and
116 then compared them with those observed from 29 September to 10 October 2004 (Fujita et al., 2008). We used dual- and
117 single-frequency carrier phase GPS receivers (GNSS Technologies, GEM-1, and MAGELLAN ProMark3). One receiver was
118 installed 2.5 km west of the terminus of Thorthormi Glacier as a reference station (Fig. 1a), whose location was determined
119 by an online precise point positioning processing service ([https://webapp.geod.nrcan.gc.ca/geod/tools-
121 outils/ppp.php?locale=en](https://webapp.geod.nrcan.gc.ca/geod/tools-
120 outils/ppp.php?locale=en), last accessed: ~~21-October-2018~~10 July 2019), which provided standard deviations of $<4 \text{ mm}$ for
122 both the horizontal and vertical coordinates after one week of continuous measurements in 2011. Observers walked on/around
123 the glaciers with a GPS receiver and antenna fixed to a frame pack. The height uncertainty of the GPS antenna during the
124 survey was $<0.1 \text{ m}$ (Tsutaki et al., 2016). The DGPS data were processed with RTKLIB, an open source software for GNSS
125 positioning (<http://www.rtklib.com/>, last accessed: ~~21-October-2018~~10 July 2019). Coordinates were projected onto a common
126 Universal Transverse Mercator projection (UTM zone 46N, WGS84 reference system). We generated 1-m DEMs by
127 interpolating the surveyed points with an inverse distance weighted method, as used in previous studies (e.g., Fujita and
128 Nuimura, 2011; Tshering and Fujita, 2016). The 2004 survey data were calibrated using four benchmarks around the glaciers
129 (Fig. 1a) to generate a 1-m DEM. Details of the 2004 and 2011 DGPS surveys, along with their respective DEMs, are
summarised in Table S1. The surface elevation changes between 2004 and 2011 were computed at points where data were

130 available for both dates. Elevation changes were obtained at 431 and 248 DEM grid points for Thorthormi and Lugge glaciers,
131 respectively (Table 1).

132 To evaluate the spatial representativeness of the change in glacier surface elevation derived from the DGPS measurements,
133 we compared the elevation changes derived from the DGPS-DEMs and Advanced Spaceborne Thermal Emission and
134 Reflection Radiometer (ASTER) DEMs acquired on 11 October 2004 and 6 April 2011 (Table S2), respectively, which cover
135 a similar period to our field campaigns (2004–2011). The 30-m ASTER-DEMs were provided by the ASTER-VA
136 (<https://gbank.gsj.jp/madas/map/index.html>, last accessed: ~~21 October 2018~~[10 July 2019](#)). The ASTER-DEM elevations were
137 calibrated using the DGPS data from the off-glacier terrain in 2011. The vertical coordinates of the ASTER-DEMs were then
138 corrected for the corresponding bias, with the elevation change over the glacier surface computed as the difference between
139 the calibrated DEMs.

140 The horizontal uncertainty of the DGPS survey was evaluated by comparing the positions of the four benchmarks installed
141 around Thorthormi and Lugge glaciers (Fig. 1a). Although previous studies utilising satellite-based DEMs have adopted the
142 standard error as the vertical uncertainty, which assumed uncorrected noise (e.g., Berthier et al., 2007; Bolch et al., 2011;
143 Maurer et al., 2016), we used the standard deviation of the elevation difference on the off-glacier terrain in the DGPS surveys,
144 which assumed systematic errors, because the large number of off-glacier points in our DGPS-DEM survey ($n = 3893$)
145 yielded an extremely small standard error. The actual horizontal uncertainty is likely the function of a noise correlated on a
146 certain spatial scale (e.g., Rolstad et al., 2009; Motyka et al., 2010).

147 **3.2 Surface flow velocities**

148 We calculated surface flow velocities by processing ASTER images (15-m resolution, near infrared, near nadir 3N band) with
149 the COSI-Corr feature tracking software (Leprince et al., 2007), which is commonly adopted in mountainous terrains to
150 measure surface displacements with an accuracy of one-fourth to one-tenth of the pixel size (e.g., Heid and Käab, 2012;
151 Scherler and Strecker, 2012; Lamsal et al., 2017). Orthorectification and coregistration of the images were performed by Japan
152 Space Systems before processing. The orthorectification and coregistration accuracies were reported as 16.9 m and 0.05 pixel,
153 respectively. We selected five image pairs from seven scenes between 22 October 2002 and 12 October 2010, with temporal
154 separations ranging from 273 to 712 days (Table S3), to obtain the annual surface flow velocities of the glaciers. It should be
155 noted that the aim of our flow velocity measurements is to investigate the mean surface flow regimes of the glaciers rather
156 than their interannual variabilities. The subpixel displacement of features on the glacier surface was recorded at every fourth
157 pixel in the orthorectified ASTER images, providing the horizontal flow velocities at 60-m resolution (Scherler et al., 2011).
158 We used a statistical correlation mode, with a correlation window size of 16×16 pixels and a mask threshold of 0.9 for noise
159 reduction (Leprince et al., 2007). The obtained ice flow velocity fields were filtered to remove residual attitude effects and
160 miscorrelations (Scherler et al., 2011; Scherler and Strecker, 2012). We applied two filters to eliminate those flow vectors with
161 large magnitude (greater than $\pm 1 \sigma$) and/or direction ($>20^\circ$) deviations from the [mean vector within the neighbouring \$21 \times 21\$](#)
162 [pixels](#).

163 ~~mean vector within the neighbouring 21 × 21 pixels.~~

164 3.3 Glacier lake area

165 We analysed ~~the areal~~-variations in the glacial lake area of Thorthormi and Lugge ~~Glaciers~~[glaciers](#) using 12 satellite images
166 acquired by the Landsat 7 ETM+ between November 2000 and December 2011 (distributed by the United States Geological
167 Survey, <http://landsat.usgs.gov/>, last accessed: ~~21 October 2018~~[10 July 2019](#)). We selected images taken in either November
168 or December with the least snow and cloud cover. We also analysed multiple ETM+ images acquired from the October to
169 December timeframe of each year to avoid the scan line corrector-off gaps. Glacial lakes were manually delineated on false
170 colour composite images (bands 3–5, 30-m spatial resolution). Following previous delineation methods (e.g., Bajracharya et
171 al., 2014; Nuimura et al., 2015; Nagai et al., 2016), marginal ponds in contact with bedrock/moraine ridge were included in
172 the glacial lake area, whereas small supraglacial ponds surrounded by ice were excluded. The accuracy of the outline mapping
173 is equivalent to the image resolution (30 m). The coregistration error in the repeated images was ±30 m, based on visual
174 inspection of the horizontal shift of a stable bedrock and lateral moraines on the coregistered imagery. The user-induced error
175 was estimated to be 5-% of the lake area delineated from the Landsat images (Paul et al., 2013). The total errors of the analysed
176 areas were less than ±0.14 and ±0.08 km² for Thorthormi and Lugge ~~Glaciers~~[glaciers](#), respectively.

177 3.4 Mass balance of the debris-covered surface

178 SMB is an essential component of ice thickness change, but no in situ SMB data are available in the Lunana region. Therefore,
179 the spatial distributions of the SMB on the debris-covered Thorthormi and Lugge glaciers were computed with a heat and mass
180 balance model, which quantifies the spatial distribution of the mean SMB for each glacier.

181 Thin debris accelerates ice melt by lowering surface albedo, while thick debris (generally more than ~5 cm) suppresses
182 ice melt and acts as an insulating layer (Østrem, 1959; Mattson et al., 1993). To obtain the spatial distributions of debris
183 thickness and SMB, we estimated the thermal resistance from remotely sensed data and reanalysis climate data (Suzuki et al.,
184 2007a; Zhang et al., 2011; Fujita and Sakai, 2014). The thermal resistance (R_T , m² K W⁻¹) is defined as follows:

185

$$186 R_T = \frac{h_d}{\lambda} \quad (1)$$

187

188 where ~~h_d~~ h_d and λ are debris thickness (m) and thermal conductivity (W m⁻¹ K⁻¹), respectively. This method has been applied
189 to reproduce debris thickness and SMB in southeastern Tibet (Zhang et al., 2011) and glacier runoff in the Nepal Himalaya
190 (Fujita and Sakai, 2014). Assuming no changes in heat storage, the linear temperature profiles within the debris layer and the
191 melting point temperature at the ice-debris interface (T_i , 0°C), the conductive heat flux through the debris layer (G_d , W m⁻²)
192 and the heat balance at the debris surface are described as follows:

193

$$194 \quad G_d = \frac{(T_s - T_i)}{R_T} = (1 - \alpha_d)R_{Sd} + R_{Ld} - R_{Lu} + H_S + H_L \quad (2)$$

195

196 where α_d is the debris surface albedo, R_{Sd} , R_{Ld} and R_{Lu} are the downward ~~short-wave~~shortwave radiation, and downward and
 197 upward ~~long-wave~~longwave radiation, respectively (positive sign, W m^{-2}), and H_S and H_L are the sensible and latent heat fluxes
 198 (W m^{-2}), respectively, which are positive when the fluxes are directed toward the ground. Both turbulent fluxes were ignored
 199 in the original method to obtain the thermal resistance, based on a sensitivity analysis and field measurements (Suzuki et al.,
 200 2007a). However, we improved the method by taking the sensible heat into account because several studies have indicated that
 201 ignoring the sensible heat can result in an underestimation of the thermal resistance (e.g., Reid and Brock, 2010). Using eight
 202 ASTER images (90-m resolution, Level 3A1 data) obtained between October 2002 and October 2010 (Table S4), along with
 203 the NCEP/NCAR reanalysis climate data (NCEP-2, Kanamitsu et al., 2002), we calculated the distribution of mean thermal
 204 resistance on the two target glaciers. The surface albedo is calculated using three visible near-infrared sensors (bands 1–3),
 205 and the surface temperature is obtained from an average of five thermal infrared sensors (bands 10–14). Automatic weather
 206 station (AWS) observations from the terminal moraine of Luggé Glacial Lake (4524 m a.s.l., Fig. 1a) showed that the annual
 207 mean air temperature was $\approx -0^\circ\text{C}$ during 2002–2004, and the annual precipitation was 900 mm in 2003 (Suzuki et al., 2007b).
 208 The air temperature at the AWS elevation was estimated using the pressure level atmospheric temperature and geopotential
 209 height (Sakai et al., 2015), and then modified for each 90×90 m mesh grid points using a single temperature lapse rate
 210 ($0.006^\circ\text{C km}^{-1}$). The wind speed was assumed to be 2.0 m d^{-1} , which is the two-year average of the 2002–2004 AWS record
 211 (Suzuki et al., 2007b). The uncertainties in the thermal resistance and albedo were evaluated as 107 and 40%, respectively, by
 212 taking the standard deviations calculated from multiple images at the same location (Fig. S2).

213 The SMB of the debris-covered ablation area was calculated by a heat and mass balance model that included debris-
 214 covered effects (Fujita and Sakai, 2014). First, the surface temperature is determined to satisfy Eq. (2) using the estimated
 215 thermal resistance and an iterative calculation, and then, if the heat flux toward the ice–debris interface is positive, the daily
 216 amount of ice melt beneath the debris mantle (M_d , $\text{kg m}^{-2} \text{ d}^{-1}$) is obtained as follows:

217

$$218 \quad M_d = \frac{t_D G_d}{l_m} \quad (3)$$

219

220 where t_D is the length of a day in seconds (86400 s) and l_m is the latent heat of fusion of ice ($3.33 \times 10^5 \text{ J kg}^{-1}$). The annual
 221 mass balance of the debris-covered part (b , m w.e. a^{-1}) is expressed as:

222

$$223 \quad b = \sum_{D=1}^{365} \left(P_s + P_r + \frac{t_D H_L}{l_m} \text{ for debris} + \frac{t_D H_L}{l_m} \text{ for snow} - D_d - D_s \right) / \rho_w \quad (4)$$

224

225 where ρ_w is the water density (1000 kg m^{-3}), P_S and P_r represent snow and rain precipitation, respectively, and D_d and D_S are
 226 the daily discharge from the debris and snow surfaces, respectively. The precipitation phase is temperature dependent, with
 227 the probability of solid/liquid precipitation varying linearly between 0 (100% snow) and 4°C (100% rain) (Fujita and Ageta,
 228 2000). Evaporation from the debris and snow surfaces is expressed in the same formula (not shown) but they are calculated in
 229 different schemes because the temperature and saturation conditions of the debris and snow surfaces are different. Discharge
 230 and evaporation from the snow surface were only calculated when a snow layer covered the debris surface. Since there is no
 231 snow layer present at either the end of [the](#) melting season in the current climate condition or at the elevation of the debris-
 232 covered area, snow accumulation (P_S) is compensated with evaporation and discharge from the snow surface during a
 233 calculation year. D_d is expressed as follow:

$$235 \quad D_d = M_d + P_r + \frac{t_D H_L}{l_m \text{ for debris}} \quad (5)$$

236
 237 which then simplifies the mass balance to:

$$239 \quad b = -\sum_{D=1}^{365} M_d / \rho_w \quad (6)$$

240
 241 This implies that the mass balance of the debris-covered area is equivalent to the amount of ice melt beneath the debris mantle.
 242 Further details on the equations and methodology used in the model are described by Fujita and Sakai (2014). The mass balance
 243 was calculated at $90 \times 90 \text{ m}$ mesh grid points on the ablation area of the two glaciers using 38 years of ERA-Interim reanalysis
 244 data (1979–2017, Dee et al., 2011), with the results given in metres of water equivalent (w.e.). The meteorological variables
 245 in the ERA-Interim reanalysis data (2002–2004) were calibrated with in situ meteorological data (2002–2004) from the
 246 terminal moraine of Lugge Glacier (Fig. S3). The ERA-Interim wind speed was simply multiplied by 1.3 to obtain the same
 247 average as in the observational data. The SMBs calculated with the observed and calibrated ERA-Interim data for 2002–2004
 248 were compared with those from the entire 38-year ERA-Interim data set. The SMBs for 2002–2004 (from both the
 249 observational and ERA-Interim data sets) show no clear anomaly against the long-term mean SMB (1979–2017) (Fig. S4).

250 The sensitivity of the simulated meltwater was evaluated against the meteorological parameters used in the SMB model.
 251 We chose meltwater instead of SMB to quantify the uncertainty because the SMB uncertainty cannot be expressed as a
 252 percentage. The tested parameters are surface albedo, air temperature, precipitation, relative humidity, solar radiation, thermal
 253 resistance and wind speed. The thermal resistance and albedo uncertainties were based on the standard deviations derived from
 254 the eight ASTER images used to estimate these parameters (Fig. S2). Each meteorological variable uncertainty, with the
 255 exceptions of the thermal resistance and albedo uncertainties, was assumed to be the root mean square error (RMSE) of the
 256 ERA-Interim reanalysis data against the observational data (Fig. S3). The simulated meltwater uncertainty was estimated as

257 the variation in meltwater within a possible parameter range via a quadratic sum of the results from each meteorological
258 parameter.

259 3.5 Ice dynamics

260 3.5.1 Model descriptions

261 To investigate the dynamically induced ice thickness change, numerical experiments were carried out by applying a two-
262 dimensional ice flow model to the longitudinal cross sections of Thorthormi and Lugge glaciers. The aim of the experiments
263 was to investigate whether the ice thickness changes observed at the glaciers were affected by the presence of proglacial lakes.

264 The model was developed for a land-terminating glacier (Sugiyama et al., 2003, 2014), and is applied to a lake-terminating
265 glacier in this study. Taking the x and z coordinates in the along flow and vertical directions, the momentum and mass
266 conservation equations in the x - z plane are:

267

$$268 \frac{\partial \sigma_{xx}}{\partial x} + \frac{\partial \sigma_{xz}}{\partial z} = 0 \quad (7)$$

269

$$270 \frac{\partial \sigma_{zx}}{\partial x} + \frac{\partial \sigma_{zz}}{\partial z} = \rho_i g \quad (8)$$

271

272 and

273

$$274 \frac{\partial u_x}{\partial x} + \frac{\partial u_z}{\partial z} = 0 \quad (9)$$

275

276 where σ_{ij} ($i, j = x, z$) are the components of the Cauchy stress tensor, ρ_i is the density of ice (910 kg m^{-3}), g is the gravitational
277 acceleration vector (9.81 m s^{-2}), and u_x and u_z are the horizontal and vertical components of the flow velocity vector,
278 respectively. The stress in Eqs. (8) and (9) is linked to the strain rate via the constitutive equation given by Glen's flow law
279 (Glen, 1955):

280

$$281 \dot{\epsilon}_{ij} = A \tau_e^{n-1} \tau_{ij} \quad (10)$$

282

283 where $\dot{\epsilon}_{ij}$ and τ_{ij} are the components of the strain rate and deviatoric stress tensors, respectively, and τ_e is the effective stress,
284 which is defined as

285

$$286 \tau_e = \frac{1}{2} (\tau_{xx}^2 + \tau_{zz}^2) + \tau_{xz}^2 \quad (11)$$

287

288 The rate factor (A , $\text{MPa}^{-3} \text{a}^{-1}$) and flow law exponent (n) are material parameters. We used the commonly accepted value of n
289 $= 3$ for the flow law exponent and employed a rate factor of $A = 75 \text{ MPa}^{-3} \text{a}^{-1}$, which was previously used to model a temperate
290 valley glacier (Gudmundsson, 1999). We assumed the glaciers were temperate. This assumption was based on a measured
291 mean annual air temperature of $\sim 0^\circ\text{C}$ ~~near on~~ the ~~front~~ terminal moraine of Lugge ~~Glacial Lake~~ Glacier (Suzuki et al., 2007b).

292 The model domain extended from 5100 m and 3500 m to the termini of Thorthormi and Lugge ~~Glaciers~~ glaciers,
293 respectively (white lines in Fig. 1b), and included the ablation and lower accumulation areas of both glaciers. We only interpret
294 the results from the ablation areas (0–~~4200~~ 4300 and ~~700–2500~~ 500–1900 m from the termini of Thorthormi and Lugge
295 ~~Glaciers~~ glaciers, respectively), with the surface flow velocities obtained from the ASTER imagery. The lower accumulation
296 area was included in the model domain to supply ice to the study region, but it was excluded from analysis of the results. The
297 surface elevation of the model domain ranges from 4443 to 4846 m for Thorthormi Glacier, and from 4511 to 5351 m for
298 Lugge Glacier. The surface geometry was obtained from the 90–m ASTER GDEM version 2 obtained in November 2001 after
299 ~~filtering~~ smoothing the elevations ~~with a smoothing routine~~ at a bandwidth of 200 m. The ice thickness distribution was
300 estimated from a method proposed for alpine glaciers (Farinotti et al., 2009), with the same rate factor ($A = 75 \text{ MPa}^{-3} \text{a}^{-1}$) ~~and~~,
301 the above-mentioned SMB model (Sect. 3.4) and satellite-based ice thickness change (Sect. 3.1). We applied the same local
302 regression filter to smooth the estimated bedrock geometry. The bedrock elevation of Thorthormi Glacier was constrained by
303 bathymetry data acquired in September 2011 at 1400 m from the terminus (red cross in Fig. 1a). For Lugge Glacier, the bed
304 elevation at the glacier front was estimated from the bathymetric map of Lugge Glacial Lake, surveyed in September 2002
305 (Yamada et al., 2004). Using the observed ice thickness data as constraints, we determined the correction factors for the method
306 of Farinotti et al. (2009) to be 0.78 and 0.36 for Thorthormi and Lugge ~~Glaciers~~ glaciers, respectively. These factors include
307 the effects of basal sliding, the geometry of the glacier cross-section, and other processes (Eq. (7) in Farinotti et al. (2009)).
308 To solve Eqs. (8) and (9) for u_x and u_z , the modelled domain was discretised with a finite element mesh. The mesh resolution
309 was 100 m in the horizontal direction, ~~and~~ several metres near the bed and 4–67 m near the surface in the vertical direction.
310 The total ~~numbers~~ number of elements were 612 and 420 for Thorthormi and Lugge glaciers, respectively. Additional
311 experiments with a finer mesh resolution confirmed convergence of ice flow velocity within 4%.

312 The glacier surface was assumed to be stress free, and the ice flux through the up-glacier model boundary was prescribed
313 from the surface velocity field obtained via the satellite analysis. ~~We assumed no basal sliding, and~~ We applied a fourth-order
314 function for the velocity profile from the surface to the bed. The basal sliding velocity (u_b) was given as a linear function of
315 the basal shear traction ($\tau_{xz,b}$):

316

$$317 \quad u_b = C_{\tau_{xz,b}}(x) \tau_{xz,b}$$

318 (12)

319

320 where C is the sliding coefficient. We used ~~constant~~spatially variable sliding coefficients ~~of $C = 356$ and $286 \text{ m a}^{-1} \text{ MPa}^{-1}$ over~~
321 ~~the entire domains of Thorthormi and Luge glaciers, respectively. These parameters, which~~ were obtained by minimising the
322 RMSE between the modelled and measured surface flow velocities ~~over the entire model domains~~within 0–4300 and 500–
323 1900 m of the termini of Thorthormi and Luge glaciers, respectively (Fig. S5).

324 3.5.2 Experimental configurations

325 To quantify the effect of glacier dynamics on ice thickness change, we performed two experiments for Thorthormi and Luge
326 ~~Glaciers~~glaciers. Experiment 1 was performed to compute the ice flow velocity fields under the present terminus conditions.
327 In this experiment, Thorthormi Glacier was treated as a land-terminating glacier with no horizontal ice motion at the glacier
328 front, whereas Luge Glacier was treated as a lake-terminating glacier by applying hydrostatic pressure at the front as a
329 function of water depth. A stress-free boundary condition was given to the calving front above the lake level. We used the
330 2001 glacier surface elevation and 2004 supraglacial pond and proglacial lake water levels as boundary conditions (Fujita et
331 al., 2008).

332 Experiment 2 was designed to investigate the influence of proglacial lakes on glacier dynamics. For Thorthormi Glacier,
333 we simulated a calving front with thickness of 125 m. The position of the hypothetical calving front was set where the lake
334 depth was acquired during a bathymetry survey in September 2011 (red cross in Fig. 1a). The surface level of the proglacial
335 lake was assumed to be 4432 m a.s.l., which is the mean surface level of the supraglacial ponds measured in September 2004
336 (Fujita et al., 2008). Hydrostatic pressure and stress-free conditions were applied to the lower boundary below and above the
337 lake level, respectively. For Luge Glacier, we simulated a lake-free situation, with ice flowing to the contemporary terminal
338 moraine, so that the glacier terminates on land. Bedrock topography is derived from the bathymetric map (white lines in Fig.
339 1b, Yamada et al., 2004). The surface topography is linearly extrapolated from the surface elevations at the calving front in
340 2002, with the ice thickness reduced to a negligibly small value at the glacier front. In the experiment, we used 444 and 684
341 elements for Thorthormi and Luge glaciers, respectively.

342 3.5.3 ~~Simulated ice thickness change~~Emergence velocity

343 To compare the influence of ice dynamics on glacier ~~thinning~~thickness change in lake- and land-terminating glaciers, we
344 calculated the emergence velocity (v_e) as follows:

$$345$$
$$346 v_e = v_z - v_h \tan \alpha \quad (13)$$
$$347$$

348 where v_z and v_h are the vertical and horizontal flow velocities, respectively, and ~~α~~ α is the surface slope (Cuffey and Paterson,
349 2010). The surface slope ~~α~~ α was obtained every 100 m from the surface topography of the ice flow model.

350 4 Results

351 4.1 Surface elevation change

352 Figure 1a shows the rates of surface elevation change ($\Delta Z_s/\Delta t$) for Thorthormi and Lugge ~~Glaciers~~glaciers from 2004 to 2011
353 derived from the DGPS-DEMs. The rates for Thorthormi Glacier range from -3.37 to $+1.14$ m a^{-1} , with a mean rate of -1.40
354 m a^{-1} (Table 1). These rates show large variability within the limited elevation band (4410–4450 m a.s.l., Fig. 2b). No clear
355 trend is observed at 1000–3000 m from the terminus (Fig. 2c). The rates for Lugge Glacier range from -9.13 to -1.30 m a^{-1} ,
356 with a mean rate of -4.67 m a^{-1} (Table 1). The most negative values (-9 m a^{-1}) are found at the lower glacier elevations (4560
357 m a.s.l., Fig. 2b), which corresponds to 1300 m from the 2002 terminus position (Fig. 2c). The RMSE between the surveyed
358 positions (five measurements in total, with one or two measurements for each benchmark) is 0.21 m in the horizontal direction.
359 The mean elevation difference between the 2004 and 2011 DGPS-DEMs is 0.48 m, with a standard deviation of 1.91 m (Fig.
360 2a), which yield an uncertainty in the elevation change rate of 0.27 m a^{-1} . The uncertainties in the elevation change rate of the
361 ASTER-DEMs are estimated to be 2.75 m a^{-1} for the 2004 and 2011 DEMs (Fig. ~~S6~~S7). Given the ASTER-DEM uncertainties,
362 the DGPS-DEMs and ASTER-DEMs yield a similar $\Delta Z_s/\Delta t$ that falls within the uncertainty ranges in the scatter plots (Figs.
363 ~~S7~~S8 and ~~S8~~S9), thus supporting the applicability of the DGPS measurements to the entire ablation area.

364 4.2 Surface flow velocities

365 Figure 1b shows the surface flow velocity field from 30 January 2007 to 1 January 2008 (337 days). On Thorthormi Glacier,
366 the flow velocities decrease down-glacier, ranging from ~ 110 m a^{-1} at the foot of the icefall to < -10 m a^{-1} at the terminus (Fig.
367 3a). The flow velocities of Lugge Glacier increase down-glacier, ranging from 20–60 to 50–80 m a^{-1} within 2000 m of the
368 calving front (Fig. 3b). The flow velocity uncertainty was estimated to be ± 12.1 m a^{-1} , as given by the mean off-glacier
369 displacement from 3 February 2006 to 30 January 2007 (362 days) (Fig. ~~S9~~S10). If these flow speeds were solely attributed
370 to ice deformation with a frozen bed assumption, ice thickness of the glaciers would be 300 to 800 m, which are much greater
371 than the bathymetry records (~ 100 m), supporting the temperate glacier assumption.

372 4.3 Changes in glacial lake area

373 The supraglacial pond area near the front of Thorthormi Glacier progressively increased from 2000 to 2011, at a mean rate of
374 0.09 $\text{km}^2 \text{ a}^{-1}$, and Lugge Glacial Lake also expanded from 2000 to 2011, at a mean rate of 0.03 $\text{km}^2 \text{ a}^{-1}$ (Fig. 4). The total area
375 changes from 2000 to 2011 were 1.79 km^2 and 0.46 km^2 for Thorthormi and Lugge glaciers, respectively.

376 4.4 Surface mass balance

377 The simulated mean SMBs over the ablation area were $-7.36 \pm 0.122.92$ m w.e. a^{-1} for Thorthormi Glacier and $-5.25 \pm$
378 ~~$0.132.41$~~ m w.e. a^{-1} for Lugge Glacier (Fig. 1c, Table 1). ~~The SMB errors are spatial variable over the calculated domains.~~ The
379 SMB distribution correlates well with the thermal resistance distribution (Fig. ~~S10~~S11), with the larger thermal resistance areas

380 suggesting a thicker debris, which results in a reduced SMB. The debris-free surface has a more negative SMB than the debris-
381 covered regions of the glaciers. The mean SMBs of the debris-free and debris-covered surfaces in the ablation area of
382 Thorthormi Glacier are $-9.31 \pm 0.683.08$ and $-7.30 \pm 0.132.96$ m w.e. a^{-1} , respectively, while those of Luge Glacier are -7.33
383 $\pm 0.412.67$ and $-5.41 \pm 0.182.53$ m w.e. a^{-1} , respectively (Table 1). The sensitivity of simulated meltwater in the SMB model
384 was evaluated as a function of the RMSE of each meteorological variable across the debris-covered area (Fig. S11 Figs. S12
385 and S13). Ice melting is more sensitive to solar radiation and thermal resistance. The influence of thermal resistance on
386 meltwater formation is considered to be small since the debris cover is thin over the glaciers. The ~~estimated~~-meltwater
387 uncertainty is ~~<estimated to be~~ $<50\%$ across most of Thorthormi and Luge glaciers (Fig. S12).

388 4.5 Numerical experiments of ice dynamics

389 The ice thinning of Luge Glacier was three times faster than that of Thorthormi Glacier. However, the mean SMB was 1.4
390 times more negative at Thorthormi Glacier, suggesting a substantial influence of glacier dynamics on ice thickness change. To
391 quantify the contribution of ice dynamics to the ice thickness change, we performed numerical experiments with the present
392 (Experiment 1) and ~~prescribed~~reversed (Experiment 2) glacier geometries.

393 4.5.1 Experiment 1 – present terminus conditions

394 Modelled results for the present geometry show significantly different flow velocity fields for Thorthormi and Luge glaciers
395 (Figs. 5c and 5d). Thorthormi Glacier flows faster (>150100 m a^{-1}) in the upper reaches, where the surface is steeper than the
396 other regions (Fig. 5c). Down-glacier of the icefall, where the glacier surface is flatter, the ice motion slows in the down-
397 glacier direction, with the flow velocities decreasing to <10 m a^{-1} near the terminus (Fig. 5e). Ice flows upward relative to the
398 surface across most of the modelled region (Fig. 5c). In contrast to the down-glacier decrease in the flow velocities at
399 Thorthormi Glacier, the computed velocities of Luge Glacier are ~~up to~~ $\sim 58 < 60$ m a^{-1} within ~~500–1500~~ $1000–1900$ m of the
400 terminus, and then increase to ~ 6590 m a^{-1} at the calving front (Fig. 5f). Ice flow is nearly parallel ~~or slightly downward~~ to the
401 glacier surface (Fig. 5d). ~~Within 900 m of the terminus of Thorthormi Glacier, the~~The modelled surface flow velocities are in
402 good agreement with the satellite-derived flow velocities (Fig. ~~within 0–4300 m of the terminus of Thorthormi Glacier (Fig.~~
403 5e). The calculated surface flow velocities of Luge Glacier agree with the satellite-derived flow velocities to $\pm 12\%$ within
404 ~~$\pm 20\%$ within 350–1850~~ $500–1900$ m (Fig. 5f).

405 4.5.2 Experiment 2 – reversed terminus conditions

406 Figure 6c shows the flow velocities simulated for the lake-terminating boundary condition of Thorthormi Glacier, in which
407 the flow velocities within 200 m of the calving front are ~ 108 times faster than those of Experiment 1 (Figs. 5c and 6c). The
408 mean vertical surface flow velocity within 2000 m of the front is still negative ($-2.611.0$ m a^{-1}). The modelled result
409 demonstrates significant acceleration as the glacier dynamics change from a compressive to tensile flow regime after proglacial
410 lake formation. For Luge Glacier, the flow velocities decrease over the entire glacier in comparison with Experiment 1 (Figs.

411 5d and 6d). The upward ice motion appears within 2500 m of the terminus. The numerical experiments demonstrate that the
412 formation of a proglacial lake causes significant changes in ice dynamics.

413 4.5.3 Simulated surface flow velocity uncertainty

414 Basal sliding accounts for ~~91-90%~~ and ~~96-91%~~ of the simulated surface flow velocities in the ablation areas of Thorthormi and
415 Lugge glaciers, respectively (Figs. 5e and 5f), suggesting that ice deformation plays a minor role in ice dynamics. The standard
416 deviations of the ASTER-derived surface flow velocities are 2.9 and 6.7 m a⁻¹ for Thorthormi and Lugge ~~Glaciers~~glaciers,
417 respectively, which are considered to be the interannual variabilities in the measured surface flow velocities (Fig. 3). We
418 performed sensitivity tests of the modelled surface flow velocities by changing the ice thickness and sliding coefficient by
419 ±30%. The results show that the simulated surface flow velocity of Thorthormi Glacier varies by ~~26-33%~~ and 51-% when the
420 ~~constant~~ sliding coefficient (C) and ice thickness are varied by ±30%, respectively (Fig. ~~S13~~S14). For Lugge Glacier, the
421 simulated flow velocity varies by ~~28-41%~~ and ~~37-39%~~ when ~~he~~the sliding coefficient and ice thickness are varied by ±30%,
422 respectively. The mean uncertainty of the simulated surface flow velocity is ~~20.7.0~~ and ~~266.9~~ m a⁻¹ for Thorthormi and Lugge
423 ~~Glaciers~~glaciers, respectively. Measured surface velocities show step changes at 800–1200 m and 1900–2000 m from the
424 termini of Thorthormi and Lugge glaciers, respectively (Fig. 3). It is likely that these step changes are due to miscorrelation in
425 feature tracking process caused by surface ogives along the centre of the glaciers. Consequently, we only interpret the simulated
426 velocities within 500–1900 m of the terminus of Lugge Glacier. For Thorthormi Glacier, we considered a mean value of
427 observed velocities at the area as a reference value of simulation.

428 ~~4.6 Simulated ice thickness change~~

429 4.6 Emergence velocity

430 Figure ~~7a~~7 shows the computed emergence velocity and SMB along the central flowlines of the glaciers. Given the computed
431 surface flow velocities from Experiment 1, the emergence velocity of Thorthormi Glacier was ~~6.89~~4.65 ± 0.3430 m a⁻¹ within
432 ~~4200~~4300 m of the terminus, ~~and increased to > 10 m a⁻¹ in the upper reaches of the glacier~~ (Fig. 7a). Conversely, the
433 emergence velocity of Luge Glacier was ~~-4.41 ± 0.83 ± 0.30~~52 m a⁻¹ within ~~700-2500~~500–1900 m of the terminus (Fig. 7a).
434 ~~Under the Experiment 1 conditions, the estimated ΔZ_s/Δt values are -2.28 ± 0.66 m a⁻¹ within 4200 m of the terminus of~~
435 ~~Thorthormi Glacier and -8.36 ± 0.73 m a⁻¹ within 700-2500 m of the calving front of Luge Glacier (Fig. 7).~~

436 The emergence velocity computed under ~~contrasting geometries~~reversed terminus conditions (Experiment 2) varies from
437 that with the present geometries (Experiment 1) for both Thorthormi and Luge glaciers. (Fig. 8). For the lake-terminating
438 condition of Thorthormi Glacier, the mean emergence velocity becomes negative (~~-2.38~~6.97 ± 0.7721 m a⁻¹) within ~~3700~~2900
439 m of the terminus. The mean emergence velocity of Luge Glacier computed with the land-terminating condition is less
440 negative (~~-0.09 ± 0.30 m a⁻¹) within 700-2500 m of the terminus. Given the same SMB distribution, the mean ΔZ_s/Δt values~~

441 are computed as $-8.02 \pm 1.10 \text{ m a}^{-1}$ for Thorthormi Glacier with the lake-terminating condition and $-7.63 \pm 0.73 \text{ m a}^{-1}$ for
442 land-terminating Lugge Glacier (Table 1). $2.00 \pm 0.52 \text{ m a}^{-1}$ within 500–1900 m of the present terminus.

443 5 Discussion

444 5.1 Glacier thinning

445 The repeat DGPS surveys revealed rapid thinning of the ablation area of Lugge Glacier between 2004 and 2011. The mean
446 $\Delta Z_S/\Delta t$ ($-4.67 \pm 0.27 \text{ m a}^{-1}$) is comparable to that for the 2002–2004 period (-5 m a^{-1} , Naito et al., 2012), whereas it is more
447 than twice as negative as that derived from the ASTER-DEMs for the 2004–2011 period ($-2.24 \pm 2.75 \text{ m a}^{-1}$). The results
448 suggest that Lugge Glacier is thinning more rapidly than neighbouring glaciers in the Nepal and Bhutan Himalayas. The mean
449 $\Delta Z_S/\Delta t$ was $-0.50 \pm 0.14 \text{ m a}^{-1}$ in the ablation area of Bhutanese glaciers for the 2000–2010 period (Gardelle et al., 2013) and
450 $-2.30 \pm 0.53 \text{ m a}^{-1}$ for debris-free glaciers in eastern Nepal and Bhutan during 2003–2009 (Kääb et al., 2012). Maurer et al.
451 (2016) reported that the mean $\Delta Z_S/\Delta t$ for Lugge Glacier during 1974–2006 ($-0.6 \pm 0.2 \text{ m a}^{-1}$) was greater than those for other
452 Bhutanese lake-terminating glaciers (-0.2 to -0.4 m a^{-1}). The mean $\Delta Z_S/\Delta t$ values of Thorthormi Glacier derived from the
453 DGPS-DEMs ($-1.40 \pm 0.27 \text{ m a}^{-1}$) and ASTER-DEMs ($-1.61 \pm 2.75 \text{ m a}^{-1}$) from 2004 to 2011 are comparable with previous
454 measurements, which range from -3 to 0 m a^{-1} for the 2002–2004 period (Naito et al., 2012). The mean rate across Thorthormi
455 Glacier was $-0.3 \pm 0.2 \text{ m a}^{-1}$ during 1974–2006 (Maurer et al., 2016), which is a typical rate in the Bhutan Himalaya.

456 Lugge Glacier is thinning more rapidly than Thorthormi Glacier, which is consistent with previous satellite-based studies.
457 For example, the $\Delta Z_S/\Delta t$ values of lake-terminating Imja and Lunding ~~Glaciers~~glaciers (-1.14 and -3.41 m a^{-1} , respectively)
458 were ~ 4 times greater than those of the land-terminating glaciers (approximately -0.87 m a^{-1}) in the Khumbu region of the
459 Nepal Himalaya (Nuimura et al., 2012). King et al. (2017) measured the $\Delta Z_S/\Delta t$ of the lower parts of nine lake-terminating
460 glaciers in the Everest area (approximately -2.5 m a^{-1}), which was 67% more negative than that of 18 land-terminating glaciers
461 (approximately -1.5 m a^{-1}). The $\Delta Z_S/\Delta t$ of lake-terminating glaciers in Yakutat ice field, Alaska (-4.76 m a^{-1}) was $\sim 30\%$
462 more negative than that of the neighbouring land-terminating glaciers (Trüssel et al., 2013).

463 5.2 Influence of ice dynamics on glacier thinning

464 ~~The modelled $\Delta Z_S/\Delta t$ values are 63 % more negative than the DGPS observations for Thorthormi Glacier and 79 % more~~
465 ~~negative than the DGPS observations for Lugge Glacier (Table 1). However, the differences in $\Delta Z_S/\Delta t$ between the two~~
466 ~~glaciers are similar; as Lugge Glacier is only 3.27 (observation) and 6.08 m a^{-1} (model) more negative than Thorthormi Glacier.~~
467 ~~The mean SMB of Thorthormi Glacier is 40% more negative than that of Lugge~~
468 Glacier. Since there is only a thin debris mantle across the ablation areas of both glaciers (Fig. S1), the more negative SMB of
469 Thorthormi Glacier could be explained by the glacier being situated at lower elevations (Fig. 2b). The modelled SMBs
470 (Thorthormi < Lugge) and observed $\Delta Z_S/\Delta t$ values (Lugge < Thorthormi) suggest that the glacier dynamics of these two

471 glaciers are substantially different. The horizontal flow velocities of Luge Glacier ~~are nearly uniform~~ increase toward the
472 terminus along the central flowline (Fig. 5d), and the computed emergence velocity is negative ($-4.41 \pm 0.83 \pm 0.3052$ m a⁻¹),
473 which means the ice dynamics accelerate glacier thinning. Conversely, the flow velocities of Thorthormi Glacier decrease
474 toward the terminus (Fig. 5c), resulting in thickening under a longitudinally compressive flow regime. The emergence velocity
475 of Thorthormi Glacier is positive ($6.894.65 \pm 0.3430$ m a⁻¹), indicating a vertically extending strain regime. ~~The calculated~~
476 ~~$\Delta z_s / \Delta t$ of Thorthormi Glacier is equivalent to 28 % of the negative SMB, implying~~ This result implies that ~~two third of the~~
477 ~~surface ablation is counterbalanced by ice dynamics. In other words,~~ dynamically induced ice thickening partly compensates
478 the negative SMB.

479 Experiment 1 demonstrates that the difference in emergence velocity between land- and lake-terminating glaciers leads to
480 contrasting thinning patterns. Furthermore, Experiment 2 demonstrates that the emergence velocity was less negative (-2.00
481 $\pm 0.09 \pm 0.3052$ m a⁻¹) in the absence of a proglacial lake at the front of Luge Glacier, ~~resulting in a decrease in the thinning~~
482 ~~rate by 9 % compared to the lake-terminating condition.~~ For Thorthormi Glacier, the emergence velocity under the lake-
483 terminating condition is negative ($-2.386.97 \pm 0.7721$ m a⁻¹), ~~resulting in a 3.5 times greater thinning rate (2.28 to 8.02 m a⁻¹;~~
484 ~~Table 1).~~ Our ice flow modelling demonstrates that dynamically induced thinning will accelerate with the development of a
485 proglacial lake at the front of Thorthormi Glacier.

486 Contrasting patterns of glacier thinning and horizontal flow velocities between land- and lake-terminating glaciers are
487 consistent with satellite-based observations over lake- or ocean-terminating glaciers and neighbouring land-terminating
488 glaciers in the Nepal Himalaya (King et al., 2017) and Greenland (Tsutaki et al., 2016). A decrease in the down-glacier flow
489 velocities over the lower reaches of land-terminating glaciers suggests a longitudinally compressive flow regime, which would
490 result in a positive emergence velocity ~~and therefore thickening to compensate for the negative SMB.~~ Conversely, for lake-
491 terminating glaciers, an increase in the down-glacier flow velocities suggests a longitudinally tensile flow regime, which would
492 yield a negative emergence velocity, resulting in ice thinning. The contrasting flow regimes modelled in this study suggest that
493 the mechanisms would not only be applicable to Thorthormi and Luge glaciers, but also to other lake- and land-terminating
494 glaciers worldwide where contrasting thinning patterns are observed. ~~The modelled thinning rates are more negative than the~~
495 ~~observed rates for both glaciers (Fig. 7b), probably~~ Quantitative evaluation of ice thickness changes is difficult from simulated
496 emergence velocities and SMB due to the uncertainties in the modelled ice thickness, basal sliding and SMB. Nevertheless,
497 our numerical experiments suggest that dynamically induced ice thickening compensates the negative SMB in the lower part
498 of land-terminating glaciers, resulting in less ice thinning compared to lake-terminating glaciers.

499 5.3 Proglacial lake development and glacier retreat

500 Luge Glacial Lake has expanded continuously and at a nearly constant rate from 2000 to 2017 (Fig. 4). Bathymetric data
501 suggest that glacier ice below the lake level accounted for 88-% of the full ice thickness at the calving front in 2001 (Fig. 5b).
502 If the lake level is close to the ice flotation level, where the basal water pressure equals the ice overburden pressure, calving
503 caused by ice flotation regulates the glacier front position (van der Veen, 1996), and the glacier could rapidly retreat (e.g.,

504 Motyka et al., 2002; Tsutaki et al., 2011). Moreover, retreat could be accelerated when the glacier terminus is situated on a
505 reversed bed slope (e.g., Nick et al., 2009). A recent numerical study estimated overdeepening of Luge Glacier within 1500
506 m of the 2009 terminus (Linsbauer et al., 2016), which could cause further rapid retreat in the future. Recent glacier inventories
507 indicate that Luge Glacier has a smaller accumulation area than Thorthormi Glacier (Nuimura et al., 2015; Nagai et al., 2016),
508 and also suggest that its smaller ice flux cannot counterbalance the ongoing ice thinning.

509 After progressive mass loss since 2000, the front of Thorthormi Glacier detached from the terminal moraine and retreated
510 further from November 2010 to December 2011 (Fig. 4a). The glacier ice was still in contact with the moraine during the field
511 campaign in September 2011, but the glacier was completely detached from the moraine on the 2 December 2011 Landsat 7
512 image. Satellite images taken after 2 December 2011 show a large number of icebergs floating in the lake, suggesting rapid
513 calving due to ice flotation. A numerical study suggested that lake water currents driven by valley winds over the lake surface
514 could enhance thermal undercutting and calving when a proglacial lake expands to a certain longitudinal length (Sakai et al.,
515 2009). A previous study estimated that the overdeepening of Thorthormi Glacier extends for >3000 m from the terminal
516 moraine (Linsbauer et al., 2016), which suggests that continued glacier thinning will lead to rapid retreat of the entire section
517 of the terminus as the ice thickness reaches flotation.

518 Experiment 2 simulates a significant increase in surface flow velocity at the lower part of Thorthormi Glacier when a
519 proglacial lake forms (Fig. 6e). Previous studies reported the speed up and rapid retreat of glaciers after detachment from a
520 terminal ridge or bedrock bump (e.g., Boyce et al., 2007; Sakakibara and Sugiyama, 2014; Trüssel et al., 2015). In addition to
521 the reduction in back stress, thinning itself decreases the effective pressure, which enhances basal ice motion and increases the
522 flow velocity (Sugiyama et al., 2011). A decrease in the effective pressure also reduces the shear strength of the water-saturated
523 till layer beneath the glacier (Cuffey and Paterson, 2010), though little information is available on subglacial sedimentation in
524 the Himalayas. Acceleration near the terminus results in ice thinning and a decrease in effective pressure, which in turn leads
525 to further acceleration of glacier flow (e.g., Benn et al., 2007b). While no clear acceleration was observed at the calving front
526 of the glacier during 2002–2011 (Fig. 3a), it is likely that the thinning and retreat of Thorthormi Glacier will accelerate in the
527 near future due to the formation and expansion of the proglacial lake.

528 **6 Conclusions**

529 To better understand the importance of glacial lake formation on rapid glacier thinning, we carried out field and satellite-based
530 measurements across lake-terminating Luge Glacier and land-terminating Thorthormi Glacier in the Lunana region, Bhutan
531 Himalaya. Surface elevations were surveyed in 2011 by DGPS across the lower parts of the glaciers and compared with a 2004
532 DGPS survey. Surface elevation changes were also measured by differencing satellite-based DEMs. The flow velocity and
533 area of the glacial lake were determined from optical satellite images. We also performed numerical experiments to
534 [quantify](#) [investigate](#) the contributions of surface mass balance (SMB) and ice dynamics in relation to the observed ice thinning.

535 Lugge Glacier has experienced rapid ice thinning which is 3.3 times greater than that observed on Thorthormi Glacier,
536 even though the modelled SMB was less negative. The numerical modelling results, using the present glacier geometries,
537 demonstrate that Thorthormi Glacier is subjected to a longitudinally compressive flow regime, suggesting that dynamically
538 induced vertical extension compensates the negative SMB, and thus results in less ice thinning than at Lugge Glacier.
539 Conversely, the computed negative emergence velocity suggests that the rapid thinning of Lugge Glacier was driven by both
540 surface melt and ice dynamics. This study reveals that contrasting ice flow regimes cause different ice thinning observations
541 between lake- and land-terminating glaciers in the Bhutan Himalaya.

542 Thorthormi Glacier has been retreating since 2000, resulting in the detachment of the glacier front from the terminal
543 moraine and the formation of a proglacial lake in 2011. Ice flow modelling with the lake-terminating boundary condition
544 indicates a significant increase in surface flow velocities near the calving front, which leads to continued glacier retreat. This
545 positive feedback will be activated in Thorthormi Glacier with the expansion of the proglacial lake, causing further thinning
546 and retreat in the near future.

547

548 **Data availability.** The ALOS satellite data are available for purchase from the Remote Sensing Technology Center of Japan
549 (<https://www.restec.or.jp/en/>). The Landsat 7 ETM+ satellite data are distributed by the United States Geological Survey
550 (<http://landsat.usgs.gov/>). ASTER-DEM data are distributed by the National Institute of Advanced Industrial Science and
551 Technology (<https://gbank.gsj.jp/madas/?lang=en>).

552

553 **Author contributions.** KF and AS designed the study. KF, JK, TN, PT, and ST conducted the field survey in 2011. KF analysed
554 the DGPS survey data in 2004 and 2011, and simulated the surface mass balance. TN calculated the satellite-based surface
555 flow velocities. SS provided ice flow models. ST analysed the data. ST and KF wrote the paper, with contributions from AS
556 and SS.

557

558 **Competing interests.** The authors declare that they have no conflict of interest.

559

560 **Acknowledgement.** We thank the Department of Geology and Mines, Bhutan, for providing the opportunity and permission to
561 conduct the field observations. We thank S. Takenaka, M. Sano, A. Sasaki, K. Ghallay and logistic members for their support
562 during the field campaign in 2011. We appreciate F. Pellicciotti, M. Truffer, and four anonymous referees for their thoughtful
563 and constructive comments. S. Tsutaki was supported by JSPS-KAKENHI (grant number 17H06104). A. Sakai was supported
564 by the Funding Program for Next Generation World Leading Researchers (NEXT Program, GR052). This research was
565 supported by the Science and Technology Research Partnership for Sustainable Development (SATREPS), supported by the
566 Japan Science and Technology Agency (JST) and the Japan International Cooperation Agency (JICA). Support was also
567 provided by JSPS-KAKENHI (grant numbers 26257202 and 17H01621).

568 **References**

- 569 Ageta, Y., Iwata, S., Yabuki, H., Naito, N., Sakai, A., Narama, C., and Karma.: Expansion of glacier lakes in recent decades
570 in the Bhutan Himalayas, *IAHS Publ.*, 264, 165–175, 2000.
- 571 Azam, M. F., Wagnon, P., Berthier, E., Vincent, C., Fujita, K., and Kargel, J. S.: Review of the status and mass changes of
572 Himalayan-Karakoram glaciers, *J. Glaciol.*, 64, 1–14, <https://doi.org/10.1017/jog.2017.86>, 2018.
- 573 Bajracharya, S. R., Maharjan, S. B., and Shrestha, F.: The status and decadal change of glaciers in Bhutan from the 1980s to
574 2010 based on satellite data, *Ann. Glaciol.*, 55(66), 159–166, <https://doi.org/10.3189/2014AoG66A125>, 2014.
- 575 Benn D., Hulton, N. R. J., and Mottram, R. H.: ‘Calving lows’, ‘sliding laws’, and the stability of tidewater glaciers, *Ann.*
576 *Glaciol.*, 46, 123–130, <https://doi.org/10.3189/172756407782871161>, 2007a.
- 577 Benn, D., Warren, C., and Mottram, R.: Calving processes and the dynamics of calving glaciers, *Earth-Sci. Rev.*, 82, 143–179,
578 <https://doi.org/10.1016/j.earscirev.2007.02.002>, 2007b.
- 579 Berthier, E., Arnaud, Y., Kumar, R., Ahmad, S., Wagnon, P., and Chevallier, P.: Remote sensing estimates of glacier mass
580 balances in the Himachal Pradesh (Western Himalaya, India), *Remote Sens. Environ.*, 108, 327–338,
581 <https://doi.org/10.1016/j.rse.2006.11.017>, 2007.
- 582 Bolch, T., Pieczonka, T., and Benn, D. I.: Multi-decadal mass loss of glaciers in the Everest area (Nepal Himalaya) derived
583 from stereo imagery, *The Cryosphere*, 5, 349–358, <https://doi.org/10.5194/tc-5-349-2011>, 2011.
- 584 Bolch, T., Kulkarni, A., Kääb, A., Huggel, C., Paul, F., Cogley, J. G., Frey, H., Kargel, J. S., Fujita, K., Scheel, M., Bajracharya,
585 S., and Stoffel, M.: The state and fate of Himalayan Glaciers, *Science*, 336, 310–314,
586 <https://doi.org/10.1126/science.1215828>, 2012.
- 587 Boyce, E. S., Motyka, R. J., and Truffer, M.: Flotation and retreat of a lake-calving terminus, Mendenhall Glacier, southeast
588 Alaska, USA, *J. Glaciol.*, 53, 211–224, <https://doi.org/10.3189/172756507782202928>, 2007.
- 589 Brun, F., Berthier, E., Wagnon, P., Kääb, A., and Treichler, D.: A spatially resolved estimate of High Mountain Asia glacier
590 mass balances from 2000 to 2016, *Nat. Geosci.*, 10, 668–673, <https://doi.org/10.1038/ngeo2999>, 2017.
- 591 Carrivick, J. L., and Tweed, F. S.: Proglacial lakes: character, behaviour and geological importance, *Quaternary Sci. Rev.*, 78,
592 34–52, <https://doi.org/10.1016/j.quascirev.2013.07.028>, 2013.
- 593 Cogley, J. G.: Glacier shrinkage across High Mountain Asia, *Ann. Glaciol.*, 57(71), 41–49,
594 <https://doi.org/10.3189/2016AoG71A040>, 2016.
- 595 Cuffey, K. M., and Paterson, W. S. B.: *The physics of glaciers*, Oxford, Butterworth-Heinemann, 2010.
- 596 Dee, D. P., Uppala, S., Simmons, A., Berrisford, P., Poli, P., Kobayashi, S., Andrae, U., Alonso-Balmaseda, M., Balsamo, G.,
597 Bauer, P., Bechtold, P., Beljaars, A., van de Berg, L., Bidlot, J.-R., Bormann, N., Delsol, C., Dragani, R., Fuentes, M., Geer,
598 A. J., Haimberger, L., Healy, S., Hersbach, H., Hólm, E. V., Isaksen, I., Kållberg, P. W., Köhler, M., Matricardi, M.,
599 McNally, A., Monge-Sanz, B. M., Morcrette, J.-J., Peubey, C., de Rosnay, P., Tavolato, C., Thépaut, J.-N., and Vitart,

600 F.: The ERA-Interim reanalysis: Configuration and performance of the data assimilation system. *Q. J. Roy. Meteorol.*
601 *Soc.*, 137, 553–597, <https://doi.org/10.1002/qj.828>, 2011.

602 Dehecq, A., Gourmelen, N., and Trouve, E.: Deriving large-scale glacier velocities from a complete satellite archive:
603 Application to the Pamir–Karakoram–Himalaya, *Remote Sens. Environ.*, 162, 55–66,
604 <https://doi.org/10.1016/j.rse.2015.01.031>, 2015.

605 Farinotti, D., Huss, M., Bauder, A., Funk, M., and Truffer, M.: A method to estimate the ice volume and ice-thickness
606 distribution of alpine glaciers, *J. Glaciol.*, 55, 422–430, <https://doi.org/10.3189/002214309788816759>, 2009.

607 Fujita, K.: Effect of precipitation seasonality on climatic sensitivity of glacier mass balance, *Earth Planet. Sci. Lett.*, 276, 14–
608 19, <https://doi.org/10.1016/j.epsl.2008.08.028>, 2008.

609 Fujita, K., and Ageta, Y.: Effect of summer accumulation on glacier mass balance on the Tibetan Plateau revealed by mass-
610 balance model, *J. Glaciol.*, 46, 244–252, <https://doi.org/10.3189/172756500781832945>, 2000.

611 Fujita, K., and Nuimura, T.: Spatially heterogeneous wastage of Himalayan glaciers, *P. Natl. Acad. Sci. USA*, 108, 14011–
612 14014, <https://doi.org/10.1073/pnas.1106242108>, 2011.

613 Fujita, K., and Sakai, A.: Modelling runoff from a Himalayan debris-covered glacier, *Hydrol. Earth Syst. Sci.*, 18, 2679–2694,
614 <https://doi.org/10.5194/hess-18-2679-2014>, 2014.

615 Fujita, K., Suzuki, R., Nuimura, T., and Sakai, A.: Performance of ASTER and SRTM DEMs, and their potential for assessing
616 glacial lakes in the Lunana region, Bhutan Himalaya, *J. Glaciol.*, 54, 220–228,
617 <https://doi.org/10.3189/002214308784886162>, 2008.

618 Fujita, K., Sakai, A., Nuimura, T., Yamaguchi, S., and Sharma, R. R.: Recent changes in Imja Glacial Lake and its damming
619 moraine in the Nepal Himalaya revealed by in situ surveys and multi-temporal ASTER imagery, *Environ. Res. Lett.*, 4,
620 045205, <https://doi.org/10.1088/1748-9326/4/4/045205>, 2009.

621 Fujita, K., Takeuchi, N., Nikitin, S. A., Surazakov, A. B., Okamoto, S., Aizen, V. B., and Kubota, J.: Favorable climatic regime
622 for maintaining the present-day geometry of the Gregoriev Glacier, Inner Tien Shan, *The Cryosphere*, 5, 539–549,
623 <https://doi.org/10.5194/tc-5-539-2011>, 2011.

624 Fujita, K., Sakai, A., Takenaka, S., Nuimura, T., Surazakov, A. B., Sawagaki, T., and Yamanokuchi, T.: Potential flood volume
625 of Himalayan glacial lakes, *Nat. Hazards Earth Syst. Sci.*, 13, 1827–1839, <https://doi.org/10.5194/nhess-13-1827-2013>,
626 2013.

627 Funk, M., and Röthlisberger, H.: Forecasting the effects of a planned reservoir which will partially flood the tongue of
628 Unteraargletscher in Switzerland, *Ann. Glaciol.*, 13, 76–81, <https://doi.org/10.1017/S0260305500007679>, 654 1989.

629 Gardelle, J., Arnaud, Y., and Berthier, E.: Contrasted evolution of glacial lakes along the Hindu Kush Himalaya mountain
630 range between 1990 and 2009, *Global Planet. Change*, 75, 47–55, <https://doi.org/10.1016/j.gloplacha.2010.10.003>, 2011.

631 Gardelle, J., Berthier, E., Arnaud, Y., and Kääh, A.: Region-wide glacier mass balances over the Pamir–Karakoram–Himalaya
632 during 1999–2011, *The Cryosphere*, 7, 1263–1286, <https://doi.org/10.5194/tc-7-1263-2013>, 2013.

633 Glen, J. W.: The creep of polycrystalline ice, *Proc. R. Soc. London, Sea. A*, 228, 519–538, <https://doi.org/10.1098/rspa>
634 1955.0066, 1955.

635 Gudmundsson, G. H.: A three-dimensional numerical model of the confluence area of Unteraargletscher, Bernese Alps,
636 Switzerland, *J. Glaciol.*, 45, 219–230, <https://doi.org/10.3198/1999JoG45-150> 219-230, 1999.

637 Heid, T., and Kääb, A.: Evaluation of existing image matching methods for deriving glacier surface displacements globally
638 from optical satellite imagery, *Remote Sens. Environ.*, 118, 339–355, <https://doi.org/10.1016/j.rse.2011.11.024>, 2012.

639 Hewitt, H., and Liu, J.: Ice-dammed lakes and outburst floods, Karakoram Himalaya: historical perspectives on emerging
640 threats, *Physical Geography*, 31, 528–551, <https://doi.org/10.2747/0272-3646.31.6.528>, 2010.

641 Huss, M., and Hock, R.: Global-scale hydrological response to future glacier mass loss, *Nature Climate Change*, 8, 135–140,
642 <https://doi.org/10.1038/s41558-017-0049-x>, 2018.

643 Immerzeel, W. W., Kraaijenbrink, P. D. A., Shea, J. M., Shrestha, A. B., Pellicciotti, F., Bierkens, M. F. P., and de Jong, S.
644 M.: High-resolution monitoring of Himalayan glacier dynamics using unmanned aerial vehicles, *Remote Sens. Environ.*,
645 150, 93–103, doi:10.1016/j.rse.2014.04.025, 2014.

646 Kääb, A.: Combination of SRTM3 and repeat ASTER data for deriving alpine glacier flow velocities in the Bhutan Himalaya,
647 *Remote Sens. Environ.*, 94, 463–474, <https://doi.org/10.1016/j.rse.2004.11.003>, 2005.

648 Kääb, A., Berthier, E., Nuth, C., Gardelle, J., and Arnaud, Y.: Contrasting patterns of early twenty-first-century glacier mass
649 change in the Himalayas, *Nature*, 488, 495–498, <https://doi.org/10.1038/nature11324>, 2012.

650 Kanamitsu, M., Ebisuzaki, W., Woollen, J., Yang, S-K., Hnilo, J. J., Fiorino, M., and Potter., G. L.: NCEP-DOE 679AMIP-
651 II Reanalysis (R-2), *B. Am. Meteorol. Soc.*, 83, 1631–1643, <https://doi.org/10.1175/BAMS-83-11-1631>, 2002.

652 King, O., Quincey, D. J., Carrivick, J. L., and Rowan, A. V.: Spatial variability in mass loss of glaciers in the Everest region,
653 central Himalayas, between 2000 and 2015, *The Cryosphere*, 11, 407–426, <https://doi.org/10.5194/tc-11-407-2017>, 2017.

654 Komori, J.: Recent expansions of glacial lakes in the Bhutan Himalayas, *Quatern. Int.*, 184, 177–186,
655 <https://doi.org/10.1016/j.quaint.2007.09.012>, 2008.

656 Lamsal, D., Fujita, K., and Sakai, A.: Surface lowering of the debris-covered area of Kanchenjunga Glacier in the eastern
657 Nepal Himalaya since 1975, as revealed by Hexagon KH-9 and ALOS satellite observations, *The Cryosphere*, 11, 2815–
658 2827, <https://doi.org/10.5194/tc-11-2815-2017>, 2017.

659 Leprince, S., Barbot, S., Ayoub, F., and Avouac, J-P.: Automatic and precise orthorectification, coregistration, and subpixel
660 correlation of satellite images, application to ground deformation measurements, *IEEE Trans. Geosci. Remote Sens.*, 45,
661 1529–1558, <https://doi.org/10.1109/TGRS.2006.888937>, 2007.

662 Linsbauer, A., Frey, H., Haeberli, W., Machguth, H., Azam, M., and Allen, S.: Modelling glacier-bed overdeepenings and
663 possible future lakes for the glaciers in the Himalaya–Karakoram region, *Ann. Glaciol.*, 57(71), 119–130,
664 <https://doi.org/10.3189/2016AoG71A627>, 2016.

665 Mattson, L. E., Gardner, J. S., and Young, G. J.: Ablation on debris covered glaciers: an example from the Rakhiot Glacier,
666 Punjab, Himalaya, IAHS Publication, 218, 289–296, 1993.

667 Maurer, J. M., Rupper, S. B., and Schaefer, J. M.: Quantifying ice loss in the eastern Himalayas since 1974 using declassified
668 spy satellite imagery, *The Cryosphere*, 10, 2203–2215, doi:10.5194/tc-10-2203-2016, 2016.

669 Mölg, T., Maussion, F., and Scherer, D.: Mid-latitude westerlies as a driver of glacier variability in monsoonal High Asia,
670 *Nature Climate Change*, 4, 68–73, <https://doi.org/10.1038/nclimate2055>, 2014.

671 Motyka, R. J., O’Neel, S., Connor, C. L., and Echelmeyer, K. A.: Twentieth century thinning of Mendenhall Glacier, Alaska,
672 and its relationship to climate, lake calving, and glacier runoff, *Global Planet. Change*, 35, 93–112,
673 [https://doi.org/10.1016/S0921-8181\(02\)00138-8](https://doi.org/10.1016/S0921-8181(02)00138-8), 2002.

674 Motyka, R. J., Fahnestock, M., and Truffer, M.: Volume change of Jakobshavn Isbræ, West Greenland: 1985–1997–2007, *J.*
675 *Glaciol.*, 56, 635–646, <https://doi.org/10.3189/002214310793146304>, 2010.

676 Nagai, H., Fujita, K., Sakai, A., Nuimura, T., and Tadono, T.: Comparison of multiple glacier inventories with a new inventory
677 derived from high-resolution ALOS imagery in the Bhutan Himalaya, *The Cryosphere*, 10, 65–85,
678 <https://doi.org/10.5194/tc-10-65-2016>, 2016.

679 Nagai, H., Ukita, J., Narama, C., Fujita, K., Sakai, A., Tadono, T., Yamanokuchi, T., and Tomiyama, N.: Evaluating the scale
680 and potential of GLOF in the Bhutan Himalayas using a satellite-based integral glacier–glacial lake inventory, *Geosciences*,
681 7, 77, <https://doi.org/10.3390/geosciences7030077>, 2017.

682 Naito, N., Suzuki, R., Komori, J., Matsuda, Y., Yamaguchi, S., Sawagaki, T., and Tshering, P.: Recent glacier shrinkages in
683 the Lunana region, Bhutan Himalayas, *Global Environ. Res.*, 16, 13–22, 2012.

684 Nick, F. M., Vieli, A., Howat, I. M., and Joughin, I.: Large-scale changes in Greenland outlet glacier dynamics triggered at the
685 terminus, *Nature Geosci.*, 2, 110–114, <https://doi.org/10.1038/ngeo394>, 2009.

686 Nie, Y., Sheng, Y., Liu, Q., Liu, L., Liu, S., Zhang, Y., and Song, C.: A regional-scale assessment of Himalayan glacial lake
687 changes using satellite observations from 1990 to 2015, *Remote Sens. Environ.*, 189, 1–13,
688 <https://doi.org/10.1016/j.rse.2016.11.008>, 2017.

689 Nuimura, T., Fujita, K., Yamaguchi, S., and Sharma, R. R.: Elevation changes of glaciers revealed by multitemporal digital
690 elevation models calibrated by GPS survey in the Khumbu region, Nepal Himalaya, 1992–2008, *J. Glaciol.*, 58, 648–656,
691 <https://doi.org/10.3189/2012JoG11J061>, 2012.

692 Nuimura, T., Sakai, A., Taniguchi, K., Nagai, H., Lamsal, D., Tsutaki, S., Kozawa, A., Hoshina, Y., Takenaka, S., Omiya, S.,
693 Tsunematsu, K., Tshering, P., and Fujita, K.: The GAMDAM glacier inventory: a quality-controlled inventory of Asian
694 glaciers, *The Cryosphere*, 9, 849–864, <https://doi.org/10.5194/tc-9-849-2015>, 2015.

695 Østrem, G.: Ice melting under a thin layer of moraine and the existence of ice cores in moraine ridges, *Geogr. Ann.*, 41, 228–
696 230, 1959.

697 Paul, F., Barrand, N. E., Berthier, E., Bolch, T., Casey, K., Frey, H., Joshi, S. P., Kononov, V., Le Bris, R., Mölg, N., Nuth,
698 C., Pope, A., Racoviteanu, A., Rastner, P., Raup, B., Scharrer, K., Steffen, S., and Winswold, S.: On the accuracy of glacier
699 outlines derived from remote sensing data, *Ann. Glaciol.*, 54(63), 171–182, <https://doi.org/10.3189/2013AoG63A296>,
700 2013.

701 Reid, T. D., and Brock, B. W.: An energy-balance model for debris-covered glaciers including heat conduction through the
702 debris layer, *J. Glaciol.*, 56, 903–916, <https://doi.org/10.3189/002214310794457218>, 2010.

703 Rolstad, C., Haug, T., and Denby, B.: Spatially integrated geodetic glacier mass balance and its uncertainty based on
704 geostatistical analysis: application to the western Svartisen ice cap, Norway, *J. Glaciol.*, 55, 666–680,
705 <https://doi.org/10.3189/002214309789470950>, 2009.

706 Sakai, A.: Glacial Lakes in the Himalayas: A Review on Formation and Expansion Processes, *Global Environ. Res.*, 16, 23–
707 30, 2012.

708 Sakai, A., and Fujita, K.: Formation conditions of supraglacial lakes on debris-covered glaciers in the Himalayas, *J. Glaciol.*,
709 56, 177–181, <https://doi.org/10.3189/002214310791190785>, 2010.

710 Sakai, A., and Fujita, K.: Contrasting glacier responses to recent climate change in high-mountain Asia, *Sci. Rep.*, 7, 13717,
711 <https://doi.org/10.1038/s41598-017-14256-5>, 2017.

712 Sakai, A., Nishimura, K., Kadota, T., and Takeuchi, N.: Onset of calving at supraglacial lakes on debris covered glaciers of
713 the Nepal Himalayas, *J. Glaciol.*, 55, 909–917, <https://doi.org/10.3189/002214309790152555>, 2009.

714 Sakai, A., Nuimura, T., Fujita, K., Takenaka, S., Nagai, H., and Lamsal, D.: Climate regime of Asian glaciers revealed by
715 GAMDAM glacier inventory, *The Cryosphere*, 9, 865–880, <https://doi.org/10.5194/tc-9-865-2015>, 2015.

716 Sakakibara, D., and Sugiyama, S.: Ice-front variations and speed changes of calving glaciers in the Southern Patagoni Icefield
717 from 1984 to 2011, *J. Geophys. Res. Earth Surface*, 119, 2541–2554, <https://doi.org/10.1002/2014JF003148>, 2014.

718 Scherler, D., and Strecker, M. R.: Large surface velocity fluctuations of Biafo Glacier, central Karakoram, at high spatial and
719 temporal resolution from optical satellite images, *J. Glaciol.*, 58, 569–580, <https://doi.org/10.3189/2012JoG11J096>, 2012.

720 Scherler, D., Bookhagen, B., and Strecker, M. R.: Hillslope glacier coupling: The interplay of topography and glacial
721 dynamics in High Asia, *J. Geophys. Res. Earth Surface*, 116, F02019, <https://doi.org/10.1029/2010JF001751>, 2011.

722 Sugiyama, S., Gudmundsson, G. H., and Helbing, J.: Numerical investigation of the effects of temporal variations in basal
723 lubrication on englacial strain-rate distribution, *Ann. Glaciol.*, 37, 49–54, <https://doi.org/10.3189/172765403781815618>,
724 2003.

725 Sugiyama, S., Skvarca, P., Naito, N., Enomoto, H., Tsutaki, S., Tone, K., Marinsek, S., and Aniya, M.: Ice speed of a calving
726 glacier modulated by small fluctuations in basal water pressure, *Nat. Geosci.*, 4, 597–600,
727 <https://doi.org/10.1038/ngeo1218>, 2011.

728 Sugiyama, S., Sakakibara, D., Matsuno, S., Yamaguchi, S., Matoba, S., and Aoki, T.: Initial field observation on Qaanaaq ice
729 cap, northwestern Greenland, *Ann. Glaciol.*, 55(66), 25–33, <https://doi.org/10.3189/2014AoG66A102>, 2014.

730 Suzuki, R., Fujita, K., and Ageta, Y.: Spatial distribution of thermal properties on debris-covered glaciers in the Himalayas
731 derived from ASTER data, *Bull. Glaciol. Res.*, 24, 13–22, 2007a.

732 Suzuki, R., Fujita, K., Ageta, Y., Naito, N., Matsuda, Y., and Karma: Meteorological observations during 2002–2004 in Lunana
733 region, Bhutan Himalayas, *Bull. Glaciol. Res.*, 24, 71–78, 2007b.

734 Trüssel, B. L., Motyka, R. J., Truffer, M., and Larsen, C. F.: Rapid thinning of lake-calving Yakutat Glacier and the collapse
735 of the Yakutat Icefield, southeast Alaska, USA, *J. Glaciol.*, 59, 149–161, <https://doi.org/10.3189/2013JoG12J081>, 2013.

736 Trüssel, B. L., Truffer, M., Hock, R., Motyka, R. J., Huss, M., and Zhang, J.: Runaway thinning of the low-elevation Yakutat
737 Glacier, Alaska, and its sensitivity to climate change, *J. Glaciol.*, 61, 65–75, <https://doi.org/10.3189/2015JoG14J125>, 2015.

738 Tshering, P., and Fujita, K.: First in situ record of decadal glacier mass balance (2003–2014) from the Bhutan Himalaya, *Ann.*
739 *Glaciol.*, 57(71), 289–294, <https://doi.org/10.3189/2016AoG71A036>, 2016.

740 Tsutaki, S., Nishimura, D., Yoshizawa, T., and Sugiyama, S.: Changes in glacier dynamics under the influence of proglacial
741 lake formation in Rhonegletscher, Switzerland, *Ann. Glaciol.*, 52(58), 31–36,
742 <https://doi.org/10.3189/172756411797252194>, 2011.

743 Tsutaki, S., Sugiyama, S., Nishimura, D., and Funk, M.: Acceleration and flotation of a glacier terminus during formation of
744 a proglacial lake in Rhonegletscher, Switzerland, *J. Glaciol.*, 59, 559–570, <https://doi.org/10.3189/2013JoG12J107>, 2013.

745 Tsutaki, S., Sugiyama, S., Sakakibara, D., and Sawagaki, T.: Surface elevation changes during 2007–13 on Bowdoin and Tugto
746 Glaciers, northwestern Greenland, *J. Glaciol.*, 62, 1083–1092, <https://doi.org/10.1017/jog.2016.106>, 2016.

747 van der Veen, C. J.: Tidewater calving, *J. Glaciol.*, 42, 375–385, doi:10.1017/S0022143000004226, 1996.

748 Ukita, J., Narama, C., Tadono, T., Yamanokuchi, T., Tomiyama, N., Kawamoto, S., Abe, C., Uda, T., Yabuki, H., Fujita, K.,
749 and Nishimura, K.: Glacial lake inventory of Bhutan using ALOS data: Part I. Methods and preliminary results, *Ann.*
750 *Glaciol.*, 52(58), 65–71, <https://doi.org/10.3189/172756411797252293>, 2011.

751 Vieli, A., and Nick, F. M.: Understanding and modelling rapid dynamic changes of tidewater outlet glaciers: issues and
752 implications, *Surv. Geophys.*, 32, 437–458, <https://doi.org/10.1007/s10712-011-9132-4>, 2011.

753 Vincent, C., Wagnon, P., Shea, J. M., Immerzeel, W. W., Kraaijenbrink, P., Shrestha, D., Soruco, A., Arnaud, Y., Brun, F.,
754 Berthier, E., and Sherpa, S. F.: Reduced melt on debris-covered glaciers: investigations from Changri Nup Glacier, Nepal,
755 *The Cryosphere*, 10, 1845–1858, <https://doi.org/10.5194/tc-10-1845-2016>, 2016.

756 Warren, C. R., and Kirkbride, M. P.: Calving speed and climatic sensitivity of New Zealand lake-calving glaciers, *Ann. Glaciol.*,
757 36, 173–178, <https://doi.org/10.3189/172756403781816446>, 2003.

758 Yamada, T., Naito, N., Kohshima, S., Fushimi, H., Nakazawa, F., Segawa, T., Uetake, J., Suzuki, R., Sato, N., Karma, Chhetri,
759 I. K., Gyenden, L., Yabuki, H., and Chikita, K.: Outline of 2002 – research activities on glaciers and glacier lakes in Lunana
760 region, Bhutan Himalaya, *Bull. Glaciol. Res.*, 21, 79–90, 2004.

761 Yao, T., Thompson, L., Yang, W., Yu, W., Gao, Y., Guo, X., Yang, X., Duan, K., Zhao, H., Xu, B., Pu, J., Lu, A., Xiang, Y.
762 Kattel, D. B., and Joswiak, D.: Different glacier status with atmospheric circulations in Tibetan Plateau and surroundings,
763 *Nature Climate Change*, 2, 663–667, <https://doi.org/10.1038/nclimate1580>, 2012.

764 Zhang, Y., Fujita, K., Liu, S. Y., Liu, Q., and Nuimura, T.: Distribution of debris thickness and its effect on ice melt at
765 Hailuoguo glacier, southeastern Tibetan Plateau, using in situ surveys and ASTER imagery, *J. Glaciol.*, 57, 1147–1157,
766 <https://doi.org/10.3189/002214311798843331>, 2011.

767 Zemp, M., Frey, H., Gärtner-Roer, I., Nussbaumer, S. U., Hoelzle, M., Paul, F., Haeberli, W., Denzinger, F., Ahlström, A. P.,
768 Anderson, B., Bajracharya, S., Baroni, C., Braun, L. N., Cáceres, B. E., Casassa, G., Cobos, G., Dávila, L. R., Delgado
769 Granados, H., Demuth, M. N., Espizua, L., Fischer, A., Fujita, K., Gadek, B., Ghazanfar, A., Hagen, J. O., Holmlund, P.,
770 Karimi, N., Li, Z. Q., Pelto, M., Pitte, P., Popovnin, V. V., Portocarrero, C. A., Prinz, R., Sangewar, C. V., Severskiy, I.,
771 Sigurðsson, O., Soruco, A., Usabaliiev, R., and Vincent, C.: Historically unprecedented global glacier decline in the early
772 21st century, *J. Glaciol.*, 61, 745–761, <https://doi.org/10.3189/2015JoG15J017>, 2015.

773

774

775

776

777

778

779

780

781

782

783

784

785

786

787

788

789

790

791

792

793

794

795

796

797

798

799 **Table 1:** Observed rate of elevation changes ($\Delta z_s/\Delta t$), calculated surface mass balance (SMB), and simulated emergence velocity (v_e) for
800 the ablation area of Thorthormi and Lugge glaciers in the Lunana region, Bhutan Himalaya. b_{ie} denotes ice-equivalent SMB.

801

Glacier		Thorthormi	Lugge
DGPS n		431	248
$\Delta z_s/\Delta t$ (m a ⁻¹)	DGPS	-1.40 ± 0.27	-4.67 ± 0.27
	ASTER	-1.61 ± 2.75	-2.24 ± 2.75
SMB (m w.e. a ⁻¹)	Ablation area	-7.36 ± 0.12 <u>2.92</u>	-5.25 ± 0.13 <u>2.41</u>
	Debris-covered area	-7.30 ± 0.13 <u>2.96</u>	-5.41 ± 0.18 <u>2.53</u>
	Debris-free area	-9.31 ± 0.68 <u>3.08</u>	-7.33 ± 0.41 <u>2.67</u>
Exp. 1 (m a ⁻¹)	b_{ie}	-8.09 ± 0.13 <u>2.93</u>	-5.77 ± 0.14 <u>2.67</u>
	v_e	+ 6.89 <u>4.65</u> ± 0.34 <u>30</u>	- 4.41 ± 0.83 0.30 <u>52</u>
Exp. 2 (m a ⁻¹)	b_{ie}	-8.09 ± 0.13 <u>2.93</u>	-5.77 ± 0.14 <u>2.67</u>
	v_e	- 2.38 <u>6.97</u> ± 0.77 <u>21</u>	- 2.00 ± 0.09 0.30 <u>52</u>

802

803

804

805

806

807

808

809

810

811

812 **Figure 1:** Glaciers and glacial lakes in the Lunana region, Bhutan Himalaya, superimposed with (a) rate of elevation change ($\Delta z_s/\Delta t$) for
 813 the 2004–2011 period derived from DGPS-DEMs, (b) surface flow velocities (arrows) with magnitude (colour scale) between 30 January
 814 2007 and 1 January 2008, and (c) simulated surface mass balance (SMB) for the 1979–2017 period. Inset map in (a) shows the location of
 815 the study site. The $\Delta z_s/\Delta t$ in (a) is depicted on a 50 m grid, which is averaged from the differentiated 1 m DEMs. Note that bathymetry of
 816 Thorthormi Lake was measured at a limited point due to icebergs (red cross). Light blue hatches indicate glacial lakes in December 2009
 817 (Ukita et al., 2011; Nagai et al., 2017). Background image is of ALOS PRISM scene on 2 December 2009. White lines in (b) indicate the
 818 central flowline of each glacier.

819

820 **Figure 2:** (a) Histogram of elevation differences over off-glacier area at 0.5 m elevation bins. The rate of elevation change for Thorthormi
 821 (blue) and Luge (red) glaciers is compared with (b) elevation in 2011, and (c) distance from the glacier termini in 2002 along the central
 822 flowlines (Fig. 1b). The red dashed line in (c) denotes the location of the calving front of Luge Glacier in 2011.

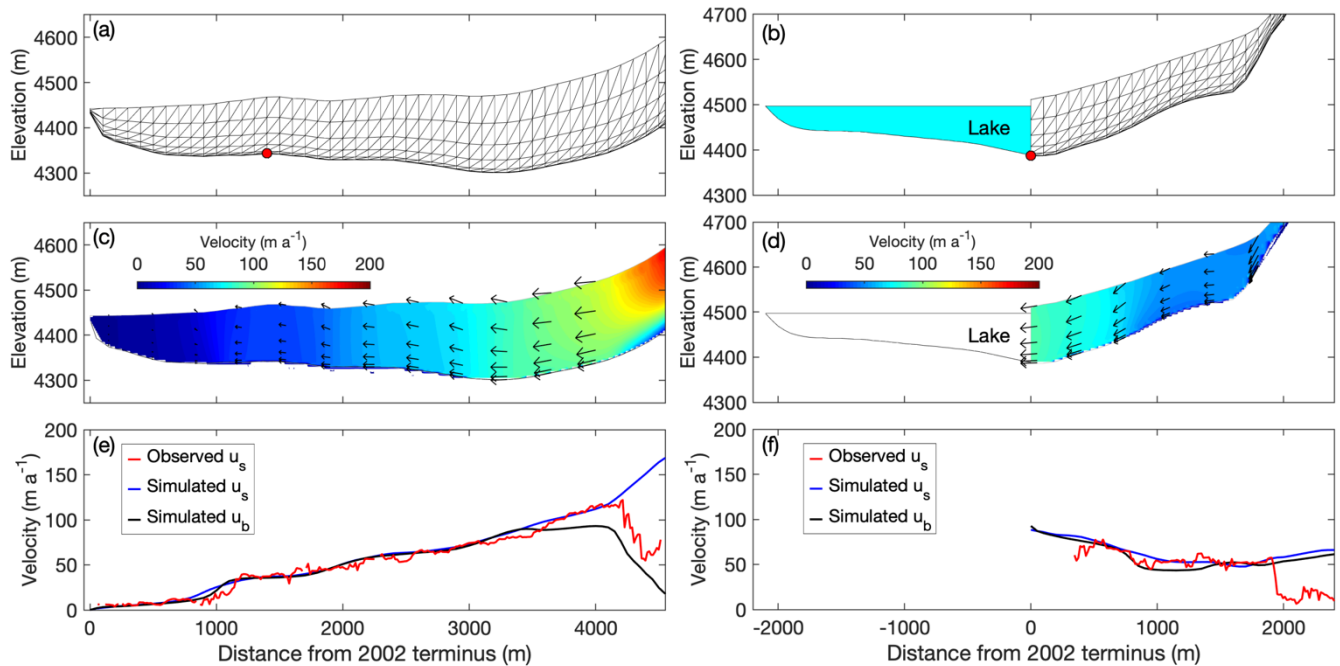
823

824 **Figure 3:** Surface flow velocities along the central flowlines of (a) Thorthormi and (b) Luge glaciers for the 2002–2010 study period. The
 825 black lines are the mean flow velocities from 2002 to 2010, with the shaded grey regions denoting the standard deviation. The distance from
 826 each respective 2002 glacier terminus is indicated on the horizontal axis.

827

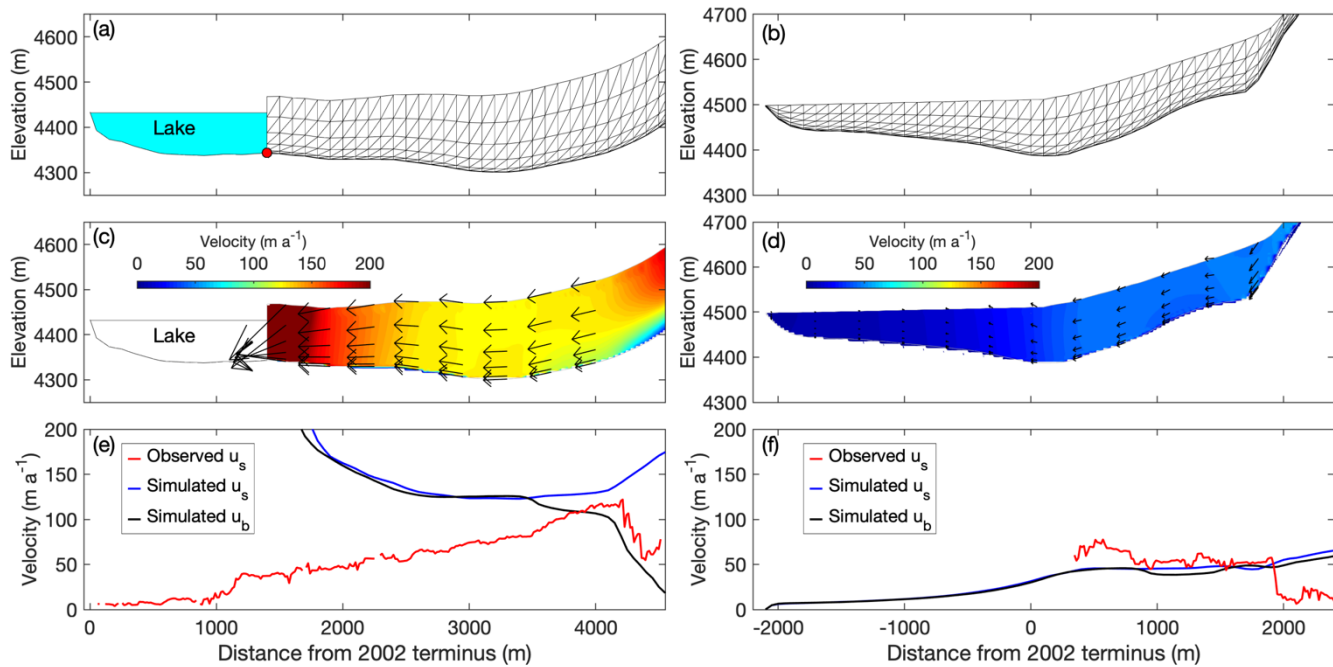
828 **Figure 4:** Glacial lake boundaries in (a) Thorthormi and (b) Luge glaciers from 2000 to 2011, and (c) cumulative lake area changes of the
 829 glaciers since 17 November 2000. The background image is an ALOS PRISM image acquired on 2 December 2009.

830



831

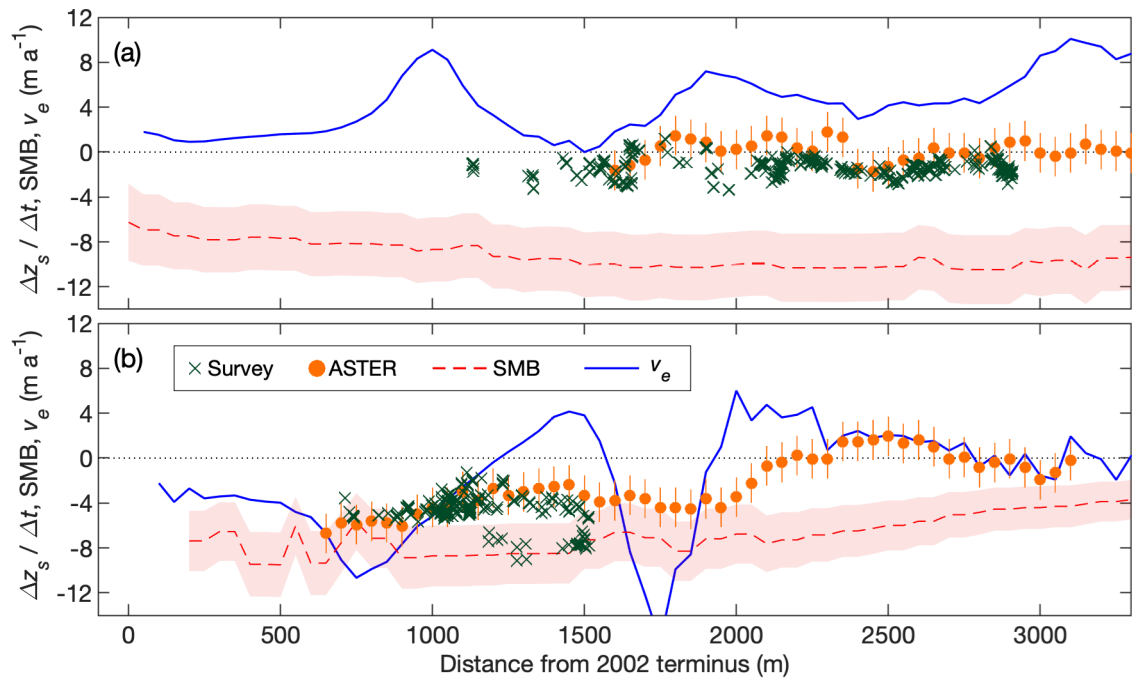
832 **Figure 5:** Ice flow simulations in longitudinal cross sections of Thorthormi (left panels) and Luge (right panels) glaciers, with the present
 833 geometries of the glaciers employed in the models. (a and b) Finite element meshes used for the simulations, with red markers indicating the
 834 bedrock elevation based on a bathymetric survey. The light blue shading in (b) indicates Luge Glacial Lake. Simulated (c and d) two-
 835 dimensional flow vectors (magnitude and direction) and (e and f) horizontal components of the flow velocity. The blue and black curves are
 836 the simulated surface (u_s) and basal velocities (u_b), respectively. The red curves are the observed surface flow velocities for 2002–2010.



837

838 **Figure 6:** Ice flow simulations in longitudinal cross sections of Thorthormi Glacier under the lake-terminating condition (left panels), and
 839 Luge Glacier under the land-terminating condition (right panels). (a and b) Finite element meshes used for the simulation. The light blue
 840 shading in (a) indicates the proglacial lake in front of Thorthormi Glacier. Simulated (c and d) two-dimensional flow vectors (magnitude
 841 and direction) and (e and f) horizontal components of the flow velocity. The blue and black curves are the simulated surface (u_s) and basal
 842 velocities (u_b), respectively. The red curves are the observed surface flow velocities for 2002–2010.

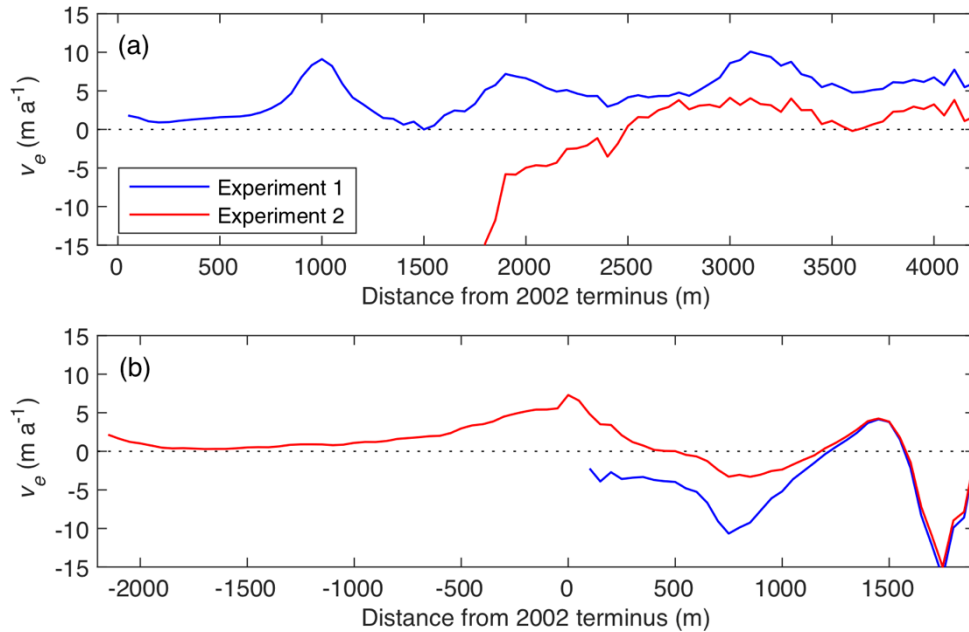
843



844

845 **Figure 7:** Rate of elevation change ($\Delta z_s / \Delta t$), from survey and ASTER-DEMs during 2004–2011, simulated surface mass balance (SMB),
 846 emergence velocity (v_e) calculations along the central flowlines of (a) Thorthormi and (b) Luge glaciers. Shaded regions denote the
 847 simulated SMB uncertainties.

848



849

850 **Figure 8:** Calculated emergence velocity (v_e) for experiment 1 and 2 along the central flowlines of (a) Thorthormi and (b) Luge glaciers.